

Politecnico di Torino

Master Degree in Physics of Complex Systems

Role of interactions in a 1-dimensional model of
stochastic transport



**Politecnico
di Torino**

Advisors:

Alessandro Pelizzola

Marco Pretti

Candidate:

Alex Panin-

forni

Academic Year 2022/2023, April Graduation Session

Contents

1	Introduction	3
2	Models	5
2.1	TASEP with open boundary conditions	5
2.2	TASEP with periodic boundary conditions	6
3	Methods	10
3.1	Cluster Mean Field: pair approximation	11
3.1.1	Introduction and numerical methods	11
3.1.2	The continuum limit	12
3.2	Kinetic Monte Carlo	17
4	Results	19
4.1	Weakly repulsive regime	21
4.2	Strongly repulsive regime	28
4.2.1	Strongly repulsive regime for $\lambda_{max} > \lambda_t$ (multi-shocks regime)	28
4.2.2	Strongly repulsive regime for $\lambda_{max} < \lambda_t$ (small shocks regime)	33
5	Conclusions	40

1 Introduction

Out of equilibrium processes, owing to their occurrences in a large number of physical phenomena that closely affect our lives, are of great relevance (think about vehicular flow or charge and heat transport). Among them, a prominent role is played by transport processes, which constitute an integral part of the most significant biological functions occurring in living beings. Indeed, at each level of organization (from intracellular environment to entire apparatuses), a lot of substances need to be transported in order to make vital processes function.

In this thesis we will discuss a model developed to deal with biological transport by means of statistical mechanics. It is worth noticing that the systems belonging to the non-equilibrium category are quite intriguing since we still do not have a well established theory to study within the statistical mechanics framework, unlike the equilibrium counterpart. For this reason, some simple models, which retain only key aspects of the processes taking place in such complex systems, has been proposed. One of the most powerful is the so called TASEP (Totally Asymmetric Simple Exclusion Process), which has been proved to be able to capture a lot of interesting aspects when applied to the study of multi-particle non-equilibrium systems, especially the ones which are well represented by one-dimensional driven motion. As a consequence, TASEP can be seen as a paradigmatic model for non-equilibrium statistical mechanics, as well as the role played by the Ising Model within equilibrium statistical mechanics.

The TASEP is defined over a one-dimensional lattice of L sites, whose sites can be empty or occupied by one particle. Particles can hop only in one direction, say rightward, from each node to the adjacent one, provided the latter is empty (as the words "totally asymmetric" and "simple exclusion" suggest).

It was proposed in 1968-69 as a stochastic model describing the kinetics of protein synthesis from mRNA via the polyribosome [1]. The polyribosome is formed by multiple ribosomes, macromolecular complexes which are capable of converting chemical energy into mechanical one by performing ATP consumption, a reaction that drives the system out of equilibrium. Ribosomes bind to a well defined codon (recall that a codon is a group of three consecutive nucleotides along the mRNA) called starting codon, then they move along the molecule always in the same direction, translating each codon into an amino acid. There are some key aspects of the dynamics of protein synthesis which explains why this process is well captured by the hypotheses of TASEP:

- The slide of ribosomes along the mRNA molecule resembles the motion of vehicles on a one-dimensional track (this kind of biological transport is indeed known as traffic-like motion) [2].
- Ribosome-mRNA coupling can only occur in a limited region identified as a codon, which can be viewed as a lattice site.
- A ribosome can move to the next codon, once the previous one has been translated, provided that there's no other ones there. Hence, their motion is subject to simple exclusion.

Remaining in the biological field, TASEP can also be implemented to mimic unidirectional cargo transport performed in the cytoplasm by kinesin and dynein, which are motor proteins "walking" on microtubule filaments and carrying cellular materials that are too massive to be driven by simple diffusion; or to deal with the movement of myosin along actin filaments responsible for muscle contraction.

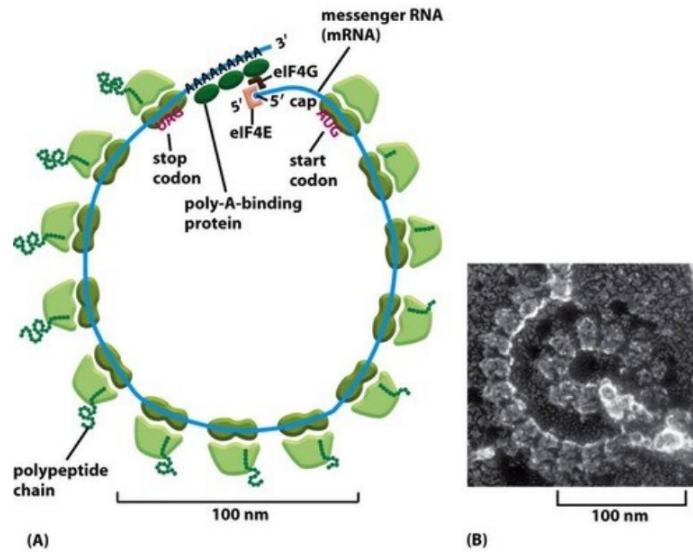


Figure 1: (A) Illustration of the polyribosome. (B) Polyribosome seen under electron microscope (Photo by John Heuser). [3]

Let us remind that even if TASEP has proved to be a valid model in describing a significant portion of this kind of systems, an exhaustive understanding of their complex dynamics cannot be explained only by means of a representation in terms of such a simple stochastic process (as an example, ribosomes take up more than one codon while performing the translation of a given triplet due to their size, so they are not well represented in this sense by a particle occupying just a single site). From this perspective, TASEP can be considered as a "minimal" model, which can be properly extended in order to provide a richer description of the peculiar system under investigation.

Following this idea, an interesting variant has been proposed for those systems for which particles are influenced by the presence of other particles in a deeper way than excluded volume principle ([4] [5] [6]). For an intuitive example, think about single file vehicular traffic: it is observed that a vehicle slows down in presence of a vehicle immediately ahead of it, and speeds up if a vehicle behind it gets closer. This feature, which can play a role as well at a microscopic level, can be included within TASEP by introducing interactions between particles, which favour or hinder the hopping of a particle depending on the occupancy of neighboring sites.

The aim of this thesis is to discuss the role of particle interactions in determining the macroscopic behaviour of an inhomogeneous system modeled by TASEP. Due to the model complexity, we will restrict to the analysis of the stationary state, whose feature is that the variables characterizing the process are assumed to be constant in time.

We are interested in the behaviour of particle density and current and how their interplay is affected by the choice of some key parameters. For this kind of systems an exact solution is not known, and so we will implement some approximate analytical methods and numerical simulations in order to find the solutions we are interested in and verify their accuracy.

2 Models

As anticipated in the introduction, TASEP is defined over a one-dimensional lattice of length L whose sites are labeled from left to right by $i = 0, \dots, L - 1$. Each of them is associated with an occupation variable n_i^t , which takes value 1 if the site i is occupied by a particle at time t and 0 if it is empty. Let us also define the local density of particles $\rho_i^t \doteq \langle n_i^t \rangle$, where $\langle \cdot \rangle$ denotes the ensemble average over multiple realizations of the stochastic process.

Neglecting the effect of the interactions for the moment, the probability per unit time of observing a particle hopping from site i to site $i + 1$ (provided the former is occupied and the latter is empty) is given by the hopping rate λ_i . In the most general case the set $\{\lambda_i\}$ is assumed to be inhomogeneous (quenched hopping rates), since the assumption of a uniform profile of rates along the lattice would not be sufficiently realistic in describing the majority of transport processes (for instance, a vehicle tends to slow down or speed up when it encounters an inhomogeneity on its trail, and this is well captured by the hypothesis that λ_i can take different values from site to site).

The two main options which have been considered in the literature for the boundary conditions are periodic and open boundary conditions. Periodic boundary conditions (referred to as PBCs) are obtained by assuming the lattice to be shaped like a ring, such that a particle at site $L - 1$ can jump into site 0, while open ones (OBCs) are obtained by assuming the lattice to be in contact with two reservoirs of particles of fixed densities. For simplicity in this thesis we will focus on the second choice, but we will provide a brief description of a simple model in which OBCs lead to some interesting results.

2.1 TASEP with open boundary conditions

In this subsection we present the simplest case of TASEP with OBCs, in which hopping rates from site i to $i + 1$ (with $i \in \{0, \dots, L - 1\}$) are all unitary and stay constant during the time evolution of the process.

Particles are injected at the leftmost site (provided it is empty) with rate α and extracted from the rightmost one (provided it is occupied) with rate β (this is completely equivalent to the previous definition if one assumes the densities of the two reservoir to be respectively equal to $\rho_l = \alpha$ and $\rho_r = 1 - \beta$, with particles injected and extracted at unit rate).

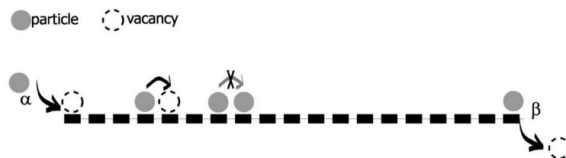


Figure 2: TASEP with open boundary conditions and unitary hopping rates, with injection rate α and extraction rate β . [7]

Notice that this could be a very schematic model of what happens in mRNA translation, with ribosomes attaching at the start codon and detaching at the stop codon.

This model is quite interesting since the behaviour of the system in the steady state reflects the behaviour of the boundaries, and a variation among the respective parameters can induce a macroscopic change in the stationary density profile which can be regarded as a phase transition. As a

consequence, one can describe a phase diagram, which is exactly known in the case of this model. In the large L limit, the stationary density profiles approach the form of a bulk solution, which is characterized by a uniform density ρ , at least sufficiently far from the boundaries. Depending on the value of α and β , the stationary state of the system can belong to three different phases. When $\alpha < \beta$ and $\alpha < 1/2$, the steady state is in a low density phase (LD), with a bulk density $\rho = \alpha < 1/2$. As we can see, the macroscopic behaviour of the system in terms of particle density is determined by what happens at the left boundary, since particles exit faster than they enter. Conversely, if $\beta < \alpha$ and $\beta < 1/2$ the state of the system corresponds to the high density phase (HD), with a bulk density $\rho = 1 - \beta > 1/2$ (particles enter faster than they exit). This is something expected if one thinks about the particle-hole symmetry characterizing this system (a particle hopping from site i to $i + 1$ can be seen exactly as a vacancy hopping from $i + 1$ to i). Eventually, when $\alpha, \beta > 1/2$, the system is found to be in the so called maximal current phase (MC), in which the bulk density is equal to $1/2$. Notice that LD and HD phases are separated by the coexistence line ($\alpha = \beta$, with $\alpha, \beta < 1/2$), over which the system displays a linear density profile, and the transition between these two phases is discontinuous. On the contrary, the transitions between low or high density phases and maximal current phase are continuous.

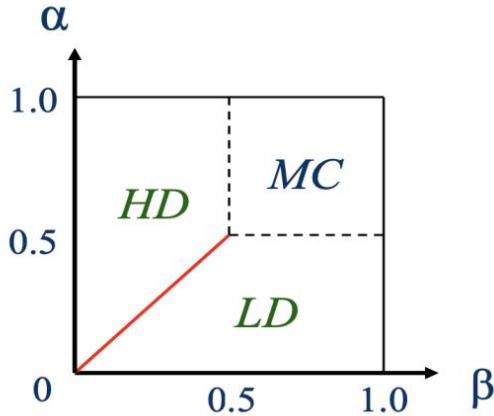


Figure 3: Phase diagram for TASEP with open boundary conditions and unitary hopping rates. [8]

2.2 TASEP with periodic boundary conditions

As reported at the end of the introduction, our main interest within this thesis is to describe the combined behaviour of interactions and spatial inhomogeneities in a TASEP model, hence we would like to avoid complications we would face by choosing open boundary conditions.

For this reason, the model over which we are going to focus is characterized by periodic boundary conditions. As anticipated, this corresponds to assuming that our 1D lattice is shaped like a ring, with site $L - 1$ connected to site 0. As a consequence, the number of particles in the initial configuration, which is denoted as $N = \sum_{i=0}^{L-1} n_i^0$, is conserved during the entire dynamics of the process.

Before moving on with our model, let us describe what happens in the simpler case of TASEP

with unitary rates when periodic boundaries are considered, since the features of the steady state can be understood quite easily in this case.

Indeed, given an initial configuration $n^0 = (n_0^0, n_1^0, \dots, n_{L-1}^0)$ such that $\sum_{i=0}^{L-1} n_i^0 = N$, one can show that all the configurations with exactly N particles have the same probability to occur in the stationary state.

Imagine to observe a generic configuration n^t at time t (with $P(n^t)$ denoting the corresponding probability) and suppose the particles in this configuration to be distributed into k clusters among the lattice. The configurations which can be reached from n^t are the ones in which a particle at the rightmost position of cluster has moved in the adjacent site, which are exactly k . Similarly, there are exactly k configurations from which n^t can be reached through a transition (which are easily constructed by starting from n^t and letting the leftmost particle of one cluster hop forward).

As a consequence, one can easily verify that the stationary state probability is a constant for the configurations with exactly N particles, and vanishes otherwise:

$$P(n^t) = \text{const} \cdot \delta_{\sum_{i=0}^{L-1} n_i, N}. \quad (1)$$

The value of the constant can be fixed by normalization if one considers the ways of distributing N particles into L sites, which amount to $\binom{L}{N} = \frac{L!}{N!(L-N)!}$. Hence

$$P(n^t) = \frac{(L-N)!N!}{L!} \delta_{\sum_{i=0}^{L-1} n_i, N}, \quad (2)$$

which verifies the stationary condition if we plug it into the corresponding master equation:

$$\frac{d}{dt} P(n^t) = k \frac{N!(L-N)!}{L!} - k \frac{N!(L-N)!}{L!} = 0. \quad (3)$$

This result allows us to compute stationary densities and correlations. Since all the sites of the lattice in the steady state have the same probability of being occupied by a particle, the probability of finding a particle at site i is given by

$$\rho \doteq \langle n_i \rangle = P(n_i = 1) = \frac{N}{L}, \quad (4)$$

which is clearly independent of the site. For what concerns the correlations, one can write

$$\langle n_i n_j \rangle = P(n_i = 1, n_j = 1) = P(n_i = 1 | n_j = 1) P(n_j = 1) = \frac{N(N-1)}{L(L-1)}, \quad (5)$$

since, given a particle at site j , the probability of finding another particle at $i \neq j$ is $(N-1)/(L-1)$. We can recursively repeat this idea in order to compute higher order correlations, whose general form reads

$$\underbrace{\langle n_i n_j \dots n_k \rangle}_{K \text{ sites}} = \prod_{l=0}^{K-1} \frac{(N-l)}{(L-l)}. \quad (6)$$

This result is quite interesting, since if one assumes to take the thermodynamic limit ($N, L \rightarrow \infty$ such that N/L remains constant) the stationary probability factors into a product of single node marginals

$$\langle n_i n_j \rangle = \rho^2, \quad \langle n_i n_j n_k \rangle = \rho^3, \quad \dots, \quad (7)$$

making the Mean Field assumption exact.
The particle current in the steady state is

$$J = \langle n_i(1 - n_{i+1}) \rangle = \rho(1 - \rho). \quad (8)$$

The plot $J(\rho)$ is known as *fundamental diagram*, and within this simple model it exhibits a single central maximum at $\rho = 0.5$, which can be regarded as an optimal value of the density (of course when $\rho = 0$ and $\rho = 1$ no current is expected since the lattice is empty and fully occupied respectively). In the following we will try to figure out how this relation is affected when some generalization of the model are considered.

As already mentioned, the insertion of interactions between particles within TASEP provides a richer description of the majority of transport phenomena, so we are going to employ nearest neighbor interactions in our model. This corresponds to including, in the expression of hopping rates, a term $\gamma(n_{i-1}, n_{i+2})$, which depends on the occupation number of sites adjacent to the ones involved in the hopping. By combining together the effect of spatial heterogeneity and interactions, the hopping rate from site i to site $i + 1$ is given by $\Gamma_i(n_{i-1}, n_{i+2}) = \lambda_i \gamma(n_{i-1}, n_{i+2})$. In order to simplify the notation, let us introduce the following parameters

$$\begin{aligned} \gamma(0,0) &= p, \\ \gamma(1,1) &= s, \\ \gamma(0,1) &= q, \\ \gamma(1,0) &= r. \end{aligned} \quad (9)$$

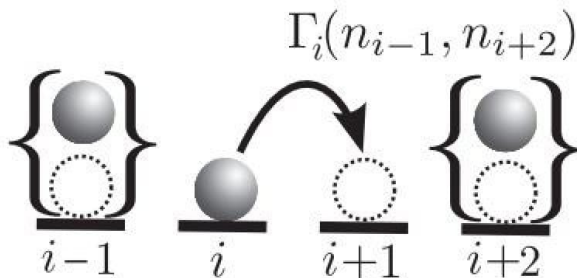


Figure 4: Sketch of particle jump with rate $\Gamma_i(n_{i-1}, n_{i+2})$ from site i to site $i + 1$ for the different possibilities of occupations of sites $i - 1$ and $i + 2$.

Notice that two interacting particles occupying neighboring sites take part to a reciprocal conditioning which can be referred as a bond, which is formed when a couple of neighboring sites becomes fully occupied and is broken when the rightmost site in the couple is left by a hopping particle. The parameters p and s describe transitions that conserve the total number of bonds, and for this reason they are generally considered to occur with equal probability among the process (notice that under the condition $p = s$ the model exhibits a particle-hole symmetry, provided rates are uniform). Under this hypothesis, typically one can set $p = s = 1$ without loss of generality, since the timescale of the process can also be fixed by a proper choice of the prefactor λ .

On the contrary, the parameters q and r are quite relevant. The first one describes how likely a

particle makes a step forward in a configuration in which a new bond is created. Similarly, the second one is related to the occurrence of a transition determining the breaking of a bond. As a consequence, $q < 1$ and $r > 1$ are expected for those kind of systems in which particles experience a repulsive interaction (and of course the opposite inequalities hold in the case of attractive interaction). In this thesis we decide to restrict the analysis to the repulsive regime, since it has been shown by other works that no changes are observed in the qualitative behaviour of the steady state of a system with attracting particles even for considerable variations of the interaction strength ([6] [9]).

3 Methods

We have used two main techniques in order to accomplish this work, which are cluster mean field approximation and kinetic Monte Carlo simulations. The combination of analytical and numerical methods allows us to enforce the understanding of the system under investigation and the interpretation of the results. Simple mean field is not adopted in this thesis since it emerged from previous studies that it is not capable of catching the majority of interesting aspects of TASEP models with interactions [6]. The most relevant feature of this model is the interplay between spatial inhomogeneity and interactions.

In the following we are going to outline some key equations referring to this class of systems.

Let us introduce the particle current from site i to $i + 1$:

$$J_i^t = \lambda_i \langle n_i^t (1 - n_{i+1}^t) [p (1 - n_{i-1}^t) (1 - n_{i+2}^t) + s n_{i-1}^t n_{i+2}^t + r n_{i-1}^t (1 - n_{i+2}^t) + q (1 - n_{i-1}^t) n_{i+2}^t] \rangle. \quad (10)$$

This expression contains an ensemble average over the sum of four terms, each of them stands for one possible particle configuration in the nodes involved in the hopping and is multiplied by the corresponding hopping rate. Notice that the four terms share a common prefactor equal to $n_i^t (1 - n_{i+1}^t)$, meaning that the hopping from node i to $i + 1$ can only occur if the first one is occupied and the latter is empty. An equivalent description can be provided in terms of joint probabilities (over the same four sites) of having a certain sequence of occupation numbers. For instance:

$$\langle n_i^t (1 - n_{i-1}^t) (1 - n_{i+1}^t) (1 - n_{i+2}^t) \rangle = P_{i-1}^t[0100], \quad (11)$$

where $P_{i-1}^t[0100]$ is the probability to observe the corresponding set of occupation variable from site $i - 1$ to $i + 2$ (in this case $n_i^t = 1$, $n_{i-1}^t = n_{i+1}^t = n_{i+2}^t = 0$). We can easily rewrite the expressions for the current by introducing four site marginals:

$$J_i^t = \lambda_i (p P_{i-1}^t[0100] + s P_{i-1}^t[1101] + q P_{i-1}^t[0101] + r P_{i-1}^t[1100]). \quad (12)$$

This expression can also be rewritten in a more compact form by exploiting the general form of the hopping rates:

$$J_i^t = \sum_{k,n=0,1} P_{i-1}^t[k10n] \Gamma_i(k, n), \quad (13)$$

where

$$\Gamma_i(0, 0) = p \lambda_i, \quad (14)$$

$$\Gamma_i(1, 1) = s \lambda_i, \quad (15)$$

$$\Gamma_i(0, 1) = q \lambda_i, \quad (16)$$

$$\Gamma_i(1, 0) = r \lambda_i. \quad (17)$$

From now on we will make the assumption $p = s = 1$ and we will mainly focus on the parameters q and r .

3.1 Cluster Mean Field: pair approximation

3.1.1 Introduction and numerical methods

Mean field cluster approximations are obtained assuming that the only relevant correlations are among clusters of at most k sites and consequently the probability distribution of the model can be approximated by a factorized form proportional to the product of k -sites marginals. Pair approximation is obtained assuming $k = 2$, hence only correlations between adjacent sites are retained. In the case of 4-sites marginals we introduced in the expression for particle currents, they can be easily expressed as a combination of 2-sites and single-site marginals under this hypothesis. More precisely:

$$P_{i-1}^t[n_{i-1}n_i n_{i+1}n_{i+2}] \cong \frac{P_{i-1}^t[n_{i-1}n_i]P_i^t[n_i n_{i+1}]P_{i+1}^t[n_{i+1}n_{i+2}]}{P_i^t[n_i]P_{i+1}^t[n_{i+1}]}.$$
 (18)

By employing this approximation into (12), with $p = s = 1$, one obtains

$$J_i^t \cong \frac{\lambda_i P_i^t[10]}{P_i^t[1]P_{i+1}^t[0]} (P_{i-1}^t[01]P_{i+1}^t[00] + P_{i-1}^t[11]P_{i+1}^t[01] + rP_{i-1}^t[11]P_{i+1}^t[00] + qP_{i-1}^t[01]P_{i+1}^t[01]).$$
 (19)

Let us also introduce the definition of local density and two-sites correlation function and their relationship with single and two nodes marginals respectively:

$$\rho_i^t \equiv P_i^t[1] = \langle n_i^t \rangle,$$
 (20)

$$1 - \rho_i^t = P_i^t[0] = \langle 1 - n_i^t \rangle,$$
 (21)

$$\phi_i^t \equiv P_i^t[11] = \langle n_i^t n_{i+1}^t \rangle.$$
 (22)

At this point, we would like to obtain a closed set of differential equations describing the time evolution of the local densities and correlations and then provide a solution by performing numerical integration. First of all, we should express the remaining two-sites marginals appearing in (19) ($P_i^t[01]$, $P_i^t[00]$ and $P_i^t[10]$) as a function of ρ and ϕ , and this can be done by exploiting the following marginalization equalities:

$$\begin{aligned} P_i^t[1] &= P_i^t[10] + P_i^t[11], \\ P_i^t[0] &= P_i^t[00] + P_i^t[01], \\ P_{i+1}^t[1] &= P_i^t[01] + P_i^t[11]. \end{aligned}$$
 (23)

Hence, combining them with equations (20-22) one obtains

$$P_i^t[10] = \rho_i^t - \phi_i^t,$$
 (24)

$$P_i^t[01] = \rho_{i+1}^t - \phi_i^t,$$
 (25)

$$P_i^t[00] = 1 - \rho_i^t - \rho_{i+1}^t + \phi_i^t.$$
 (26)

Replacing each marginal in the local current expression, we eventually obtain the desired form

$$J_i^t \cong \frac{\lambda_i (\rho_i^t - \phi_i^t)}{\rho_i^t (1 - \rho_{i+1}^t)} [(\rho_i^t - \phi_{i-1}^t) (1 - \rho_{i+1}^t - \rho_{i+2}^t + \phi_{i+1}^t) + \phi_{i-1}^t (\rho_{i+2}^t - \phi_{i+1}^t) + r\phi_{i-1}^t (1 - \rho_{i+1}^t - \rho_{i+2}^t + \phi_{i+1}^t) + q(\rho_i^t - \phi_{i-1}^t) (\rho_{i+2}^t - \phi_{i+1}^t)].$$
 (27)

The dynamics of the local densities is described by the discretized form of the continuity equation

$$\dot{\rho}_i^t = J_{i-1}^t - J_i^t. \quad (28)$$

Unfortunately, these last two equations by themselves do not form a closed system of equations. Hence, it's necessary to inspect also the time evolution of ϕ_i^t , which is given by the following Master equation:

$$\dot{\phi}_i^t = \sum_{k=0,1} P_{i-2}^t[k101]\Gamma_{i-1}(k, 1) - \sum_{n=0,1} P_i^t[110n]\Gamma_{i+1}(1, n). \quad (29)$$

If we exploit now the pair approximation and we replace the 2-nodes marginals with formulas from (24) to (26), the last equation becomes

$$\begin{aligned} \dot{\phi}_i^t \cong & \frac{(\rho_{i-1}^t - \phi_{i-1}^t)(\rho_{i+1}^t - \phi_i^t)\lambda_i}{\rho_{i-1}^t(1 - \rho_i^t)} ((\rho_{i-1}^t - \phi_{i-2}^t)q + \phi_{i-2}^t) + \\ & - \frac{\phi_i^t(\rho_{i+1}^t - \phi_{i+1}^t)\lambda_{i+2}}{\rho_{i+1}^t(1 - \rho_{i+2}^t)} ((1 - \rho_{i+2}^t - \rho_{i+3}^t + \phi_{i+2}^t)r + (\rho_{i+3}^t - \phi_{i+2}^t)). \end{aligned} \quad (30)$$

If we combine this expression with equations (27) and (28), we have finally obtained a closed set of equations in the corresponding set of variables (ρ^t, ϕ^t) .

As anticipated, the main idea is to approximate the time behaviour of our system through a computer algorithm which numerically solves our equations. Suppose to know the complete set of ρ and ϕ variables at a given time t . The structure of the algorithm is the following:

1. Compute the value of each local current J_i^t using (27).
2. Compute the value of local densities and probabilities at the next time step using a discrete time version of equations (28) and (30). More explicitly:

$$\rho_i^{t+\Delta} = \rho_i^t + \Delta (J_{i-1}^t - J_i^t), \quad (31)$$

and same for the update of ϕ .

3. Repeat these two steps until convergence.

To determine at which time step the system is sufficiently close to the stationary state, we define a parameter $\xi = \Delta^{-1} \|\rho^t - \rho^{t-\Delta}\|$ (where $\|\cdot\|$ denotes the maximal single point difference between the two profiles ρ^t and $\rho^{t-\Delta}$) and we stop the algorithm when ξ stays below a proper threshold.

Moreover, we have to chose a proper initialization (ρ^0, ϕ^0) which reproduces the required average density. There are many possible choices that ensure the convergence of the algorithm to the stationary state and the simplest one is to set each local density to the average value ($\rho_i^0 = N/L \forall i$). For what concerns the initialization of ϕ , consistently with the previous statement, we have chosen to set $\phi_i^0 = (N/L)^2$ (notice that this can be considered as the assumption that the system does not experience any correlation at the initial time, and so $\phi_i^0 = \rho_i^0 \rho_{i+1}^0$).

3.1.2 The continuum limit

A typical simplifying assumption for this kind of model is to assume that the set of hopping factors $\{\lambda_i\}$ with $i = 0, \dots, L-1$ is described by a piecewise continuous, smooth and slowly varying function $\lambda(\frac{i}{L})$. Let us also introduce a new variable $x = \frac{i}{L}$ in order to label sites, which becomes a continuous variable between 0 and 1 in the hydrodynamic limit $L \rightarrow \infty$ [6].

The choice of the shape of this function is not crucial in determining the qualitative behavior of the system we are going to describe, but it has to necessarily exhibit a single absolute minimum (in the absence of this assumption there are some complications we will not consider within this work [10]). These hypotheses suggest us to look for the non-equilibrium stationary state of our system in the form of a bulk solution (these assumptions about the form of the steady state will be denoted as bulk hypotheses in the following), so we can drop all time and site indices in the marginals appearing in our set of equations (actually within this framework the analytical density and correlations become functions which are expected to share the same properties we described for $\lambda(x)$, and so they can be considered approximately constant on a local level [11]).

It can be shown that the stationary current can be expressed in a quite simple form

$$J = \lambda(x)f(\rho(x); r, q). \quad (32)$$

This formula describes the bulk current-density relation, in which f does not depend explicitly on the spatial coordinate x . Furthermore, the qualitative behaviour of f is strongly affected by the parameters regulating the interactions. By considering a value of q in the interval $(0, \frac{1}{3})$, if the rate r becomes stronger than a given thresholding value, f begins to exhibit two lateral symmetric maxima instead of a single central one (Figure 5), and this aspect is crucial for what concerns the analytical solutions for $\rho(x)$. We are going to provide a more detailed description of this statement in the following.

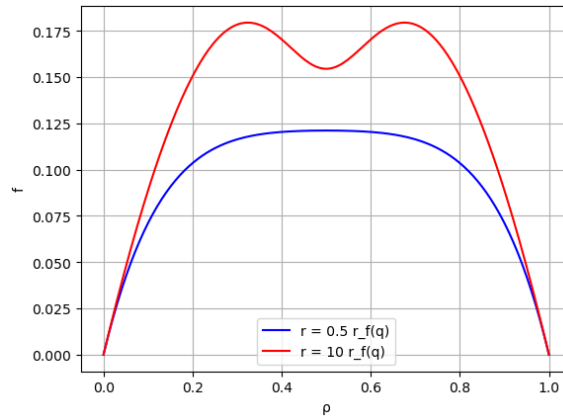


Figure 5: Bulk current-density relation for $q = 0.05$ with r below (blue) and above (red) the threshold.

By introducing the pair approximation (notice that, as a consequence of the approximation of local homogeneity, one has $P[10] = P[01]$), we can write the particle current as

$$J = \lambda(x) \frac{P[10]}{P[1]P[0]} (P[10] (P[00] + P[11]) + qP[10]) + rP[00]P[11]. \quad (33)$$

Similarly to what we have done in the previous subsection, let us express single site marginals in terms of the bulk density

$$\begin{aligned} P[1] &= \rho, \\ P[0] &= 1 - \rho, \end{aligned} \quad (34)$$

and introduce some useful marginalization equalities (Kolmogorov conditions):

$$P[10] + P[11] = \rho, \quad (35)$$

$$P[10] + P[00] = 1 - \rho. \quad (36)$$

Let us also introduce the correlator η , which will become very useful in the next steps:

$$\eta \equiv \frac{P[10]}{\rho(1-\rho)}. \quad (37)$$

Using equations (34 - 37), one can write the remaining 2-site marginals as

$$\begin{aligned} P[10] &= \eta\rho(1-\rho), \\ P[00] &= (1-\eta\rho)(1-\rho), \\ P[11] &= [1-\eta(1-\rho)]\rho. \end{aligned} \quad (38)$$

The dynamics of the correlation under the bulk hypotheses is described by the following master equation

$$\dot{\phi} = \sum_{k=0,1} P[k101]\Gamma(k,1) - \sum_{n=0,1} P[110n]\Gamma(1,n). \quad (39)$$

Since in our case $\Gamma(0,0) = \Gamma(1,1) = \lambda$, $\Gamma(0,1) = q\lambda$ and $\Gamma(1,0) = r\lambda$, the terms corresponding to $k=1$ and $n=1$ in the two sums are equivalent and cancel out.

By imposing the steady state condition $\dot{\phi} = 0$ and the pair approximation, the latter reduces to

$$\frac{P[11]P[00]}{P[10]^2} = \frac{q}{r}. \quad (40)$$

This condition can be turned into a useful equation for η using (38):

$$\frac{1}{\eta^2} - \frac{1}{\eta} + I \left[1 - \frac{q}{r} \right] = 0. \quad (41)$$

in which we have introduced $I = \rho(1-\rho)$ (since our system preserves particle-hole symmetry, the current only depends on the product of ρ and $1-\rho$). By replacing (38) into (33) and taking into account (41), one eventually obtains

$$J = \lambda r \left[2\eta I \frac{1-q}{r-q} + (1-\eta) \left(\frac{r+q-2qr}{(r-q)^2} \right) \right]. \quad (42)$$

As mentioned before, if the hopping parameter r becomes sufficiently strong with respect to q , a changing in the shape of the bulk current-density relation is observed, with the appearance of two symmetric maxima and a central local minimum. As a consequence, there is a continuous interval of I values in the proximity of the boundary $I = 0.25$ over which the function $J(I)$ is decreasing (the latter is clearly increasing if it has a single central maximum when expressed in terms of ρ). Then, one can find the critical value $r_f(q)$ determining the transition between the two regimes by observing for which value of r the slope of the function $J(I)$ evaluated in $I = 0.25$ changes sign (Figure 6).

Thus, by setting $\frac{dJ}{dI}|_{I=0.25} = 0$ (also taking into account that η depends on I), one obtains

$$r_f(q) = \frac{q(q+1)^2}{(3q-1)^2}, \quad (43)$$

which describes a continuous transition line in the (q, r) plane with $q \in (0, \frac{1}{3})$ (notice that this expression includes also a branch of curve for $q > \frac{1}{3}$ which is a spurious solution).

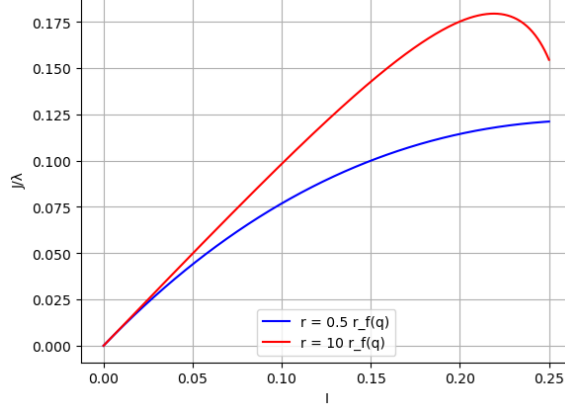


Figure 6: $\frac{J(I)}{\lambda}$ in the two regimes.

Let us focus on the analytical solutions for the density profiles $\rho(x)$ at fixed current. In this case, it can be easily shown from equation (42) that $\frac{1}{\eta}$ is a linear function of I . Then, by replacing this function into (41) one obtains a second order polynomial equation in I

$$\frac{\lambda r (\alpha I - \beta)}{J - \beta \lambda r} \left[\frac{\lambda r (\alpha I - \beta)}{J - \beta \lambda r} - 1 \right] + I \left(1 - \frac{q}{r} \right) = 0, \quad (44)$$

in which we have introduced $\alpha = \frac{2(1-q)}{r-q}$ and $\beta = \frac{r+q-2rq}{(r-q)^2}$.

We would like to compare the solutions of this equation with the results we obtain by performing numerical integration and KMC simulations, so we would mainly consider the inversion under the maximal value of the current (as we can see from (32), $J_{max} = \lambda_{min} f_{max}$, where $f_{max} = \max_{\rho \in [0,1]} f(\rho; r, q)$), given that most of the profiles we are interested in describing exhibit this current value.

The polynomial has two solutions $I_{1,2}$ in the case $r > r_f(q)$, which corresponds to four density profiles once performed the inversion $\rho_{\pm}(I) = \frac{1}{2} (1 \pm \sqrt{1 - 4I})$, while for $r < r_f(q)$ the two solutions collapse into a single one.

Before moving on with the description of the results, let us point out some significant aspects about the function $\lambda(x)$ describing the profile of the rates along the lattice.

In order to accomplish this work we adopted a sinusoidal function for the rates, whose explicit expression is

$$\lambda(x) = \frac{\lambda_{min} + \lambda_{max}}{2} + \frac{\lambda_{max} - \lambda_{min}}{2} \cos(2\pi x), \quad (45)$$

with $\lambda_{max} > \lambda_{min}$. This function exhibits a minimum for $x = 0.5$ (with $\lambda(0.5) = \lambda_{min}$) and two maxima for $x = 0$ and $x = 1$ (with $\lambda(0) = \lambda(1) = \lambda_{max}$), which are actually a single maximum

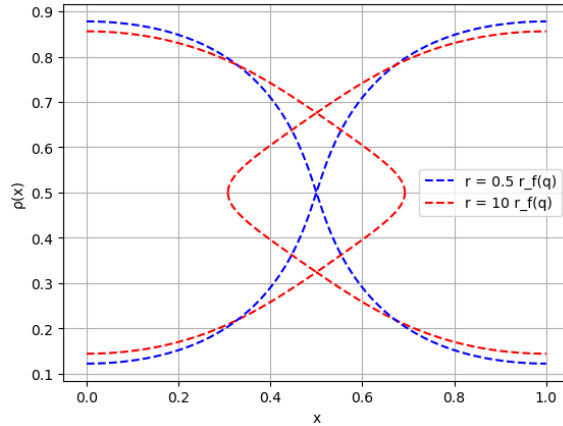


Figure 7: Analytical solutions for $\rho(x; J_{max})$ in the two regimes.

taking into account PBCs. As one can see from Figure 7, the intermediate solutions of the analytical density profiles (corresponding to the inversion of I_2) exist only for a range of values of x sufficiently close to the midpoint of the interval $[0, 1]$. Nevertheless, one can show that, given the parameters q and r such that $r > r_f(q)$, there is a critical value of the ratio $\lambda_{max}/\lambda_{min}$ (which will be denoted as $\lambda_t \equiv \lambda_t(q, r)$) below which the intermediate solutions extends over all the interval $[0, 1]$ (see Figure 8b), and this plays a fundamental role in determining the qualitative behaviour of the stationary density profiles. For simplicity in the following we will always consider $\lambda_{min} = 1$ and consider variations of λ_{max} (under this assumption the previous condition reduces to $\lambda_{max} < \lambda_t$).

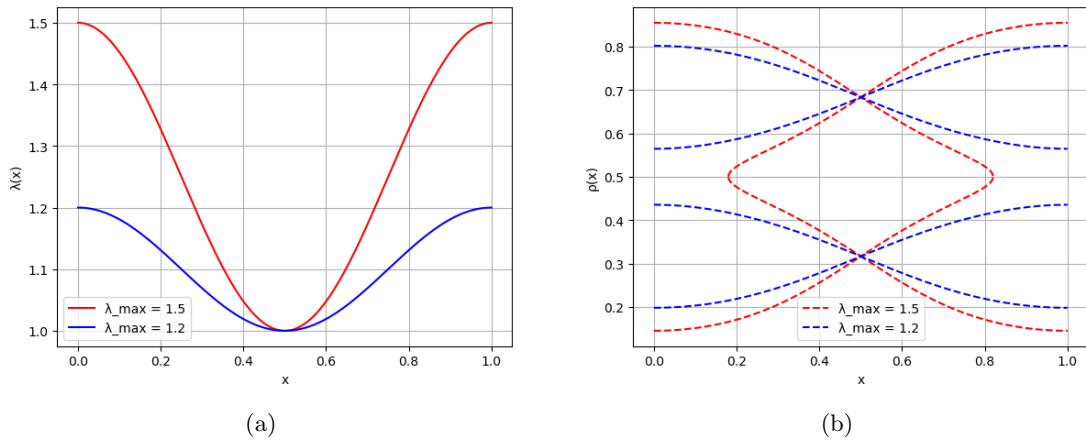


Figure 8: (a) Profiles for $\lambda(x)$ corresponding to $\lambda_{min} = 1$ for two different values of λ_{max} . (b) Analytical density profiles for $\lambda_{max} > \lambda_t$ (red) and $\lambda_{max} < \lambda_t$ (blue) with $q = 0.05$, $r = 1.95$, $\lambda_{min} = 1$ and $\lambda_t(q, r) = 1.35648$.

3.2 Kinetic Monte Carlo

This technique (also known as Gillespie algorithm [12]) aims at describing, in a stochastic manner, those systems for which the transition rates between the states are known. Our system is well represented by a continuous time Markov chain and so this simulation method is clearly suitable for our purposes.

Suppose the system to be in a well known configuration at an initial time $t = 0$ and let's call this configuration $n^0 = (n_0^0, \dots, n_{L-1}^0)$. In order to move the system forward in time it is sufficient to determine how long it will take to get to the next configuration and which one will be eventually reached. Moreover, since all the allowed transitions in our system involve the hopping of a particle from a given site i to the next one, the transition rate W_i between the two corresponding states coincides with the hopping rate $\Gamma_i(n_{i-1}, n_{i+2})$. Hence the probability that the next transition is the hopping from $i - 1$ to i and occurs in the infinitesimal time interval $(t + \tau, t + \tau + d\tau)$, given n^t at time t , is $P(\tau, i)d\tau$ which can be written as

$$P(\tau, i)d\tau = P_0(\tau)d\tau W_i, \quad (46)$$

where $P_0(\tau)$ is the probability that no transition occurs in $(t, t + \tau)$ and t is the time of the last transition. Notice that one can easily obtain the expression for $P_0(\tau)$ by splitting the time interval $(t, t + \tau)$ into n sub-intervals with amplitude $d\tau = \frac{\tau}{n}$ and by considering the probability of having no transition among all the sub-intervals. In the limit $n \rightarrow \infty$, this reduces to a Poissonian:

$$P_0(\tau) = \left(1 - \frac{\tau}{n} \sum_{l=0}^{L-1} W_l\right)^n \rightarrow e^{-\tau \sum_{l=0}^{L-1} W_l}, \quad (47)$$

implying that

$$P(\tau, i) = W_i e^{-\tau \sum_{l=0}^{L-1} W_l}. \quad (48)$$

At this point one wants to obtain a pair (τ, k) from a set described by the probability density $P(\tau, k)$, and this can be done by performing the Inverse Transform Sampling. It consists in generating two random numbers ϵ_1 and ϵ_2 from the unit-interval uniform distribution, and then by computing

$$\tau = -\frac{1}{\sum_{l=0}^{L-1} W_l} (\epsilon_1), \quad (49)$$

$$\sum_{l=0}^{k-1} W_l < \epsilon_2 \sum_{l=0}^{L-1} W_l \leq \sum_{l=0}^k W_l. \quad (50)$$

The computer algorithm implementing this method consists into four main steps:

1. Set the initial time t at 0 and define a maximum number of transitions T and an initial configuration n^0 such that $n_i^0 = 0, 1$ and $\sum_{i=0}^{L-1} n_i^0 = N$. Assign also the rates $W_i = \Gamma_i(n_{i-1}, n_{i+2})$.
2. Generate a random number ϵ_1 , compute τ with the previous formula and update the time to the value $t + \tau$.
3. Generate a random number ϵ_2 and look for the k satisfying the inequalities in (50). The transition involves a hopping from site $k - 1$ to site k . Notice that each transition rate W_i is equal to zero if $(n_{i-1}, n_i) \neq (1, 0)$, so this method ensures the hopping to occur from an occupied site to an empty one.

4. Update the occupation variables associated with the two sites involved in the hopping and all the transition rates referring to the sites in their neighborhood. At this point, the algorithm returns to the second step and performs this cycle of operation until it reaches the established number of transitions.

The density of particles of each site is computed as a weighted time average over the corresponding occupation variables computed before each transition, where the weight is given by the time occurred until the next transition

$$\rho_i = \sum_{j=T_0}^{T-1} \frac{n_i^{t_j} (t_{j+1} - t_j)}{t_{T-1} - t_{T_0}}. \quad (51)$$

As often happens in this kind of simulation, the sum doesn't start from the first transition since the initial configuration may be widely different from the expected stationary profile. Hence, in order to prevent the measurement to be conditioned by the transient to the steady state, a thermalization time T_0 is introduced, which is set to $0.05T$ after proper testing.

4 Results

In this section we are going to discuss the results we obtained by inspecting the stationary state density profiles of the model by means of the methods we have introduced previously.

We are mainly interested in the behaviour of the system in the hydrodynamic limit, so in principle we would like to send the number of lattice sites L to infinity. This is clearly not possible in practice since the computational effort which is involved would become too great, anyway L can be chosen large enough to prevent our result from being exceedingly conditioned by finite size effects while keeping a reasonable computation time. We decide to consider $L = 2000$ for most of the results we are going to describe (for both numerical CMF and KMC), but in some specific cases we will consider a higher value of L (which will be always stated explicitly) in order to minimize the effect of finite size and provide a deeper understanding of the outcomes (especially in the case of simulations, that are more affected by the limited size of the system). Actually, when the numerical CMF is implemented, one may consider values of the size for which the stationary profiles are indistinguishable from the hydrodynamic limit (at our images scale), without excessively increasing the computation time. However, we decide to evaluate the two methods at the same size in order to provide a more direct comparison between them (we will see in the following that numerical profiles obtained with CMF for $L = 4000$ and $L = 8000$ are pretty close, therefore the latter can be intended as a good estimate of the infinite-size result).

Since our model preserves at any time the number of particles filling the lattice at the beginning of the process (due to our choice of the boundary conditions), in order to catch the entire phenomenology of the model for a given choice of the parameters we have to find the corresponding stationary density profiles for different values of the average density n (which can be regarded as a control parameter of our process).

Notice that, since our system preserves particle-hole symmetry, it is sufficient to consider $n \in [0.5, 1]$, since the profiles corresponding to the complementary values of n can be easily obtained by employing a symmetry transformation. More precisely, given the average density $n \in [0.5, 1]$ with the respective solution $\rho_\beta(x)$, the profile corresponding to the average density $1 - \beta$ is given by $\rho_{1-\beta}(x) = 1 - \rho_\beta(1 - x) \forall x$ (Figure 9).

As anticipated, our theoretical analysis predicts two different behaviours of the system depending on the values of the parameters q and r .

We will first discuss the steady state of the system in the regime in which two analytical solutions (which will be denoted as $\rho_\pm(x)$) are expected. As we described in the previous section, this corresponds to the region of the (q, r) plane obeying to $r < r_f(q)$, and for this reason we will denote this regime as "weakly repulsive". In order to better understand how interactions affect the steady state within this framework, we will also report the results obtained by assuming $q = 1$, $r = 1$, corresponding to the case in which particles become non-interacting (of course excluding the hard-core repulsion).

Then we will move on to the "strongly repulsive" region ($r > r_f(q)$), for which our theory predicts four different solutions ($\rho_{1,\pm}(x)$ and $\rho_{2,\pm}(x)$).

A typical procedure which has been frequently adopted in the literature involves assuming q and r to be not independent. Since the two parameters are proportional to the probability of observing a particle hop in which a bond is broken or created respectively, one of the main ideas is to consider these two processes as descriptive of opposite chemical reactions, so they have to fulfill the detailed balance condition. Hence, if one assumes that neighboring particles interact with an energy

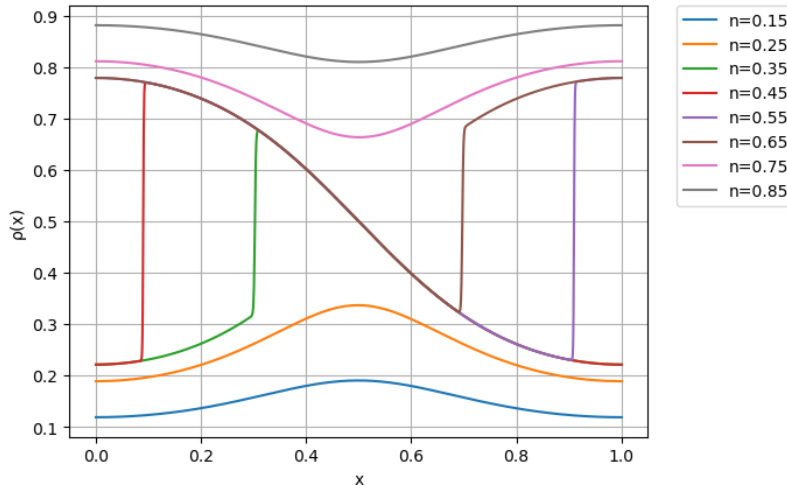


Figure 9: Stationary density profiles obtained for $q = 0.5$ and $r = 1.5$ for different values of the average density n . Notice the symmetry between the profiles with $n < 0.5$ and $n > 0.5$.

E (which is negative in the case of repulsive particles), this corresponds to setting $q/r = e^E$ (leading to $r = 1/q$ if one assumes that the energy E is equally split between creation and breaking processes) [13].

In this work we adopt another choice which is of great relevance since it has been shown that under this condition an exact bulk current-density relation can be obtained for this model under the assumption of a uniform profile of the rates. This corresponds to assuming that our rates satisfy the following relation (which is known in the literature as KLS condition) [5]

$$p + s - q - r = 0. \quad (52)$$

Since in our case $p = s = 1$, the latter implies $q + r = 2$, which means $r = 2 - q$. Notice that this condition does not restrict our analysis to a trivial case since we are able to explore both the interesting regimes (weakly and strongly repulsive) moving on this line (see Figure 10). We would like to understand if under this assumption a theory in which the pair approximation is employed is suitable to describe the system also in the presence of spatial inhomogeneities.

Let us finally remind that all the results we are going to describe have been obtained by implementing the two computer algorithms we introduced in Section 3.1 and 3.2. For what concerns the cluster mean field numerical solutions, we decide to set the ξ value for which the system has reached the steady state to 10^{-9} since in all the cases we analyzed we did not observe any sensible changes by lowering further the threshold value. On the contrary, while implementing Kinetic Monte Carlo simulations, we do not choose a well defined value of T (even if we always consider $T > 10^8$) and in each situation we look for the best compromise between lowering the noise and keeping a reasonable computation time (notice that the noise level is inversely proportional to the average number of transitions per site).

In the following we will be interested in some cases in evaluating the steady state current J . When the system reaches the stationary state, the density at each site remains constant in time, implying $\dot{\rho}_i = 0 \quad \forall i$. According to the continuity equation, one expect $J_i = J_{i+1} \quad \forall i$, which means that the

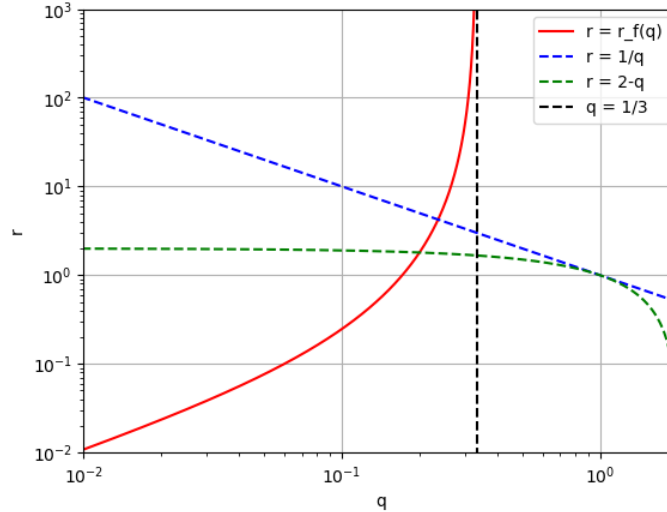


Figure 10: The two discussed relations between r and q . As we can see, the related functions span both the weakly and strongly repulsive regimes.

current is uniform along the lattice ($J_i = J \ \forall i$). The algorithm which numerically solves the set of equations in the pair approximation updates the values of the set of currents $\{J_i\}$ at each time steps until the termination condition is fulfilled, while the Gillespie algorithm computes each currents by considering the number of times a particle hopped in the corresponding site per unit of time. In both cases, one eventually obtains a set of L values of J_i which are almost identical. Hence, we decide to consider the average of the set as the steady state current, in formulae:

$$J \doteq \frac{\sum_{i=0}^{L-1} J_i}{L}. \quad (53)$$

4.1 Weakly repulsive regime

Let us start by considering the case in which the particles experience a little repulsion. In this case we have chosen to set $q = 0.5$, which implies $r = 1.5$.

For a sufficiently high value of the average density n , the density profiles of the steady state are described by a spatially smoothly varying and symmetric function with a minimum in $x = 0.5$, which takes values higher than the intermediate density $\rho = 0.5$ along the entire interval $[0, 1]$ (see Figure 11a). As a consequence, one refers to this class of solutions as the high density smooth phase (*HD*). By symmetry, the same qualitative behaviour is observed if the average density becomes sufficiently small, for which one identifies the corresponding low density smooth phase (*LD*) (Figure 11b).

These two phases are characterized by a growth of steady state current J as the average density n moves towards the intermediate value 0.5, and the shape of the fundamental diagram $J(n)$ can be obtained by performing numerical integration of the analytical solution $\rho_{\pm}(x; J)$ (from which we compute the average density n) computed for a set of values of J in the interval $(0, J_{max})$, with $J_{max} = \lambda_{min} f_{max} = 0.27452$.

If the average density becomes lower than a given value (which will be denoted as n_+), the system is found in a new phase, with different features with respect to the smooth phase (notice that the

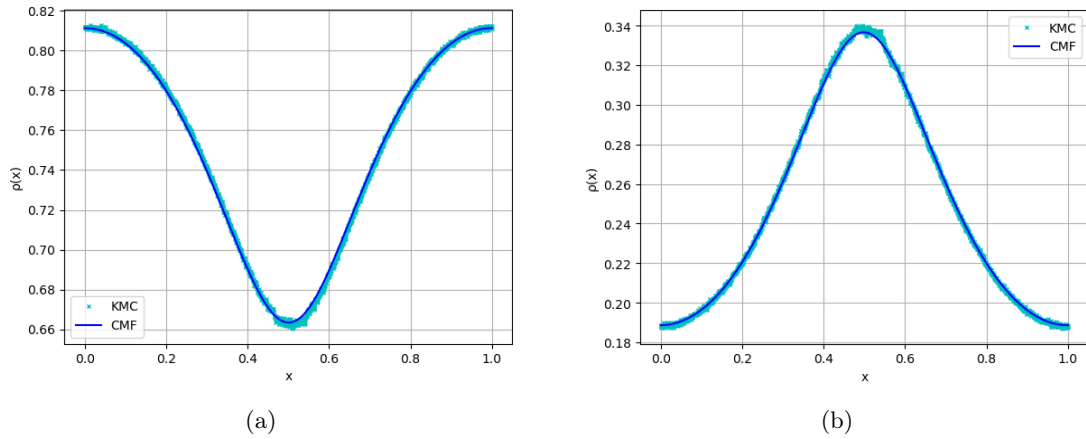


Figure 11: Stationary density profiles in the *HD* smooth phase for $n = 0.75$ (a) and in the *LD* one, for $n = 0.25$ (b).

same happens by increasing the average density above a low density value $n_- = 1 - n_+$). Actually density profiles are no longer symmetric and are characterized by the presence of a domain wall (also called shock), which corresponds to a jump from a density value typical of the low density phase to a high density one. For these reasons, this phase is called "shock phase" and from a physical point of view is characterized by the coexistence of a low density phase with a high density one (let us remind that this phenomenology is well known in the literature and it has been previously pointed out in other works, in particular [10]).

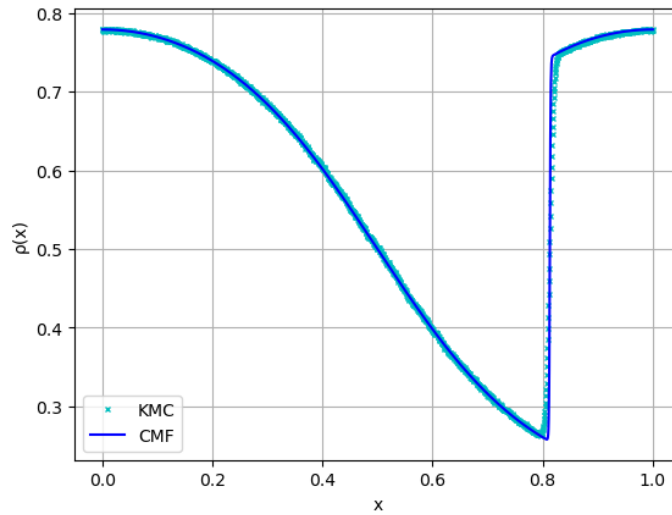


Figure 12: Stationary density profile in the shock phase for $n = 0.6$.

As one can see from Figure 12, the shock is not perfectly vertical in the profile obtained through the

simulation and this is a consequence of the limited size of the system. By increasing L the transition becomes steeper and tends progressively to a true discontinuity (see Figure 13).

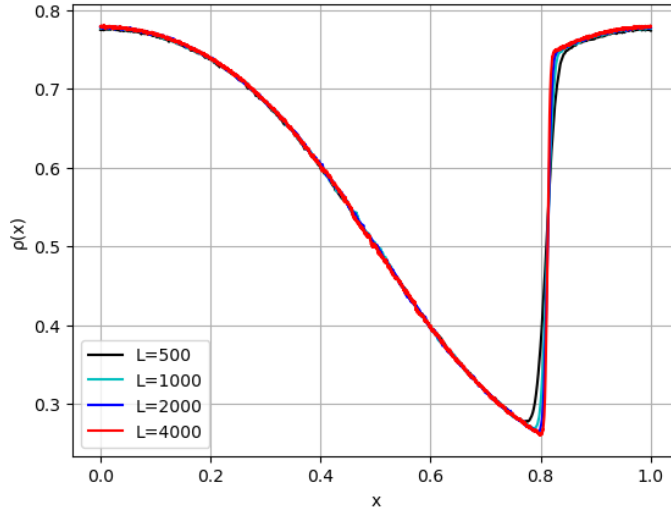


Figure 13: Comparison between the profiles obtained with KMC for different values of L .

At odds with the smooth phase, the value of the steady state current does not depend on the value of the average density, and one observes $J = J_{max}$ for $n_- < n < n_+$ (Figure (14)).

KMC simulations are in agreement with the theoretical predictions about the current behaviour in the two phases, even if the corresponding current values are larger than J_{max} , which is an effect of finite size. Indeed, by increasing L , the results of simulations become progressively closer to the analytical value of the maximal current.

The different behaviour of the system in the two phases can be clearly understood by comparing the profiles we obtain from numerical integration and simulations with the analytical ones. In the following description, we will denote as $\rho_n(x)$ the stationary profile corresponding to an average density n . Let us compute the value of stationary current J obtained for $n = 0.75$, for which the system is found in the HD smooth phase (one gets $J = 0.24269$), and then evaluate $\rho_{\pm}(x; J)$. If we compare the solution $\rho_+(x; J)$ with the stationary profiles we obtained in Figure 11a, we observe a perfect correspondence (Figure 15).

Notice that in this particular case the solutions refer to a current whose value is not maximal, hence $\rho_+(x; J)$ and $\rho_-(x; J)$ do not cross at $x = 0.5$ as in the previous plots, for which we always considered $J = J_{max}$.

On the contrary, when the average density becomes lower than n_+ , the stationary density profiles are given by a combination of $\rho_+(x; J_{max})$ and $\rho_-(x; J_{max})$, giving rise to the shock phase we mentioned above (Figure 16).

The position of the shock slides rightward along the x axis as the average density decreases in order to extend the region over which the stationary profile $\rho(x)$ coincides with the analytical solution $\rho_-(x; J_{max})$ (Figure 17).

Indeed, due to particle conservation, it must hold

$$\int_0^1 \rho_n(x) dx = n. \quad (54)$$

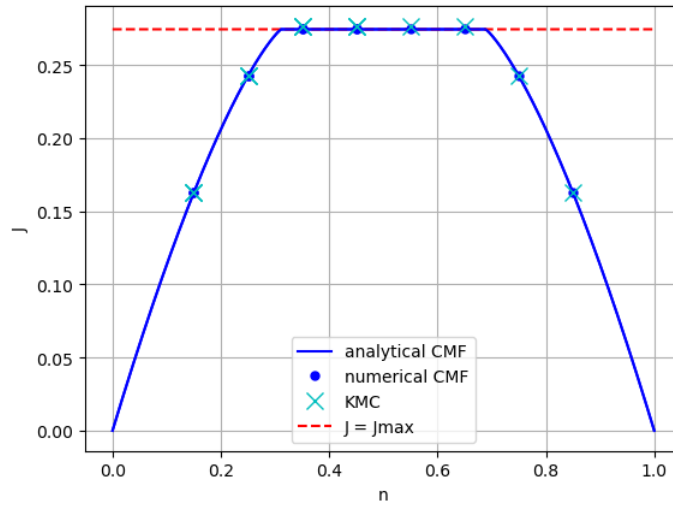


Figure 14: Comparison between the fundamental diagram obtained by integration of the analytical solutions with the values of the current obtained through the numerical algorithm solving equations in the pair approximation (numerical CMF) and KMC simulations for different values of the average density n .

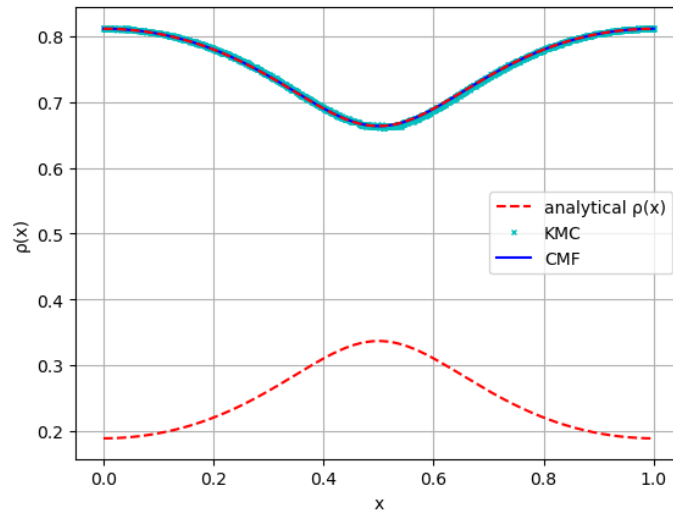


Figure 15: Comparison between the profile obtained with finite-size numerical solution and analytical solutions for $n = 0.75$ and $J = 0.24269$.

This condition allows us to compute the explicit value of n_+ , since at the boundary between the HD smooth phase and the shock phase one observes $J = J_{max}$, but the profile still coincides with

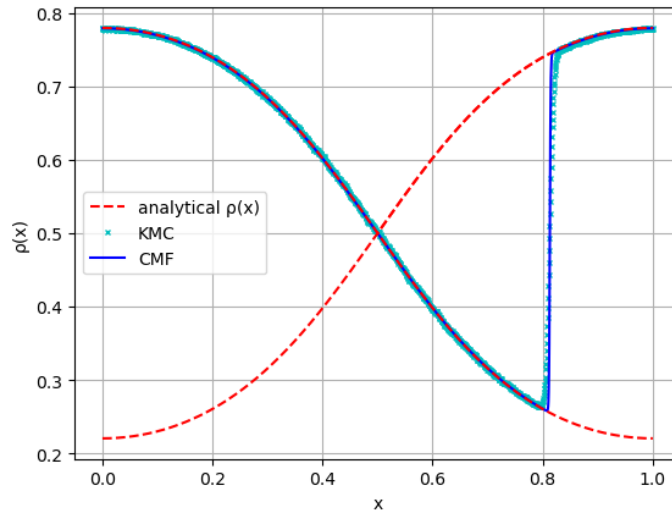


Figure 16: Comparison between the profile obtained with finite-size numerical solution and analytical solutions for $n = 0.6$ and $J = J_{max} = 0.27451$.

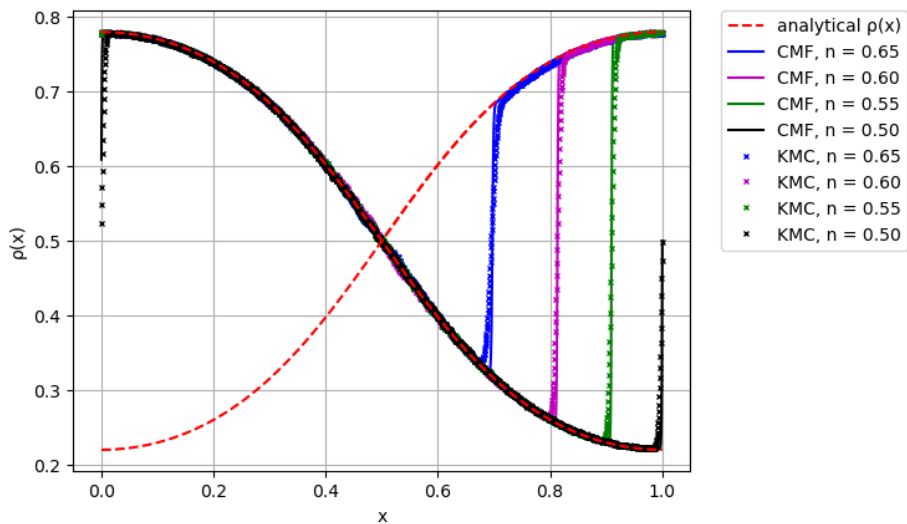


Figure 17: Plot of some stationary profiles in the shock phase obtained with the two different methods with the analytical solutions under the assumption of maximal current. Notice that by lowering the average density n the shock move towards higher values of x .

the solution $\rho_+(x; J_{max})$. More explicitly

$$n_+ = \int_0^1 \rho_{n_+}(x) dx = \int_0^1 \rho_+(x; J_{max}) dx. \quad (55)$$

For a given choice of the parameters q and r , the explicit value of n_+ depends on the ratio $\lambda_{max}/\lambda_{min}$ (hence, provided $\lambda_{min} = 1$, it depends on the value of λ_{max}). The effect of increasing the maximal value of the function $\lambda(x)$ is to increase the range of values of the average density for which the system is found in the shock phase (hence, the value of n_+ increases with λ_{max}). This allows us to build a diagram in the (λ_{max}, n) plane which can be intended as a phase diagram referring to the weakly repulsive regime (Figure 18).

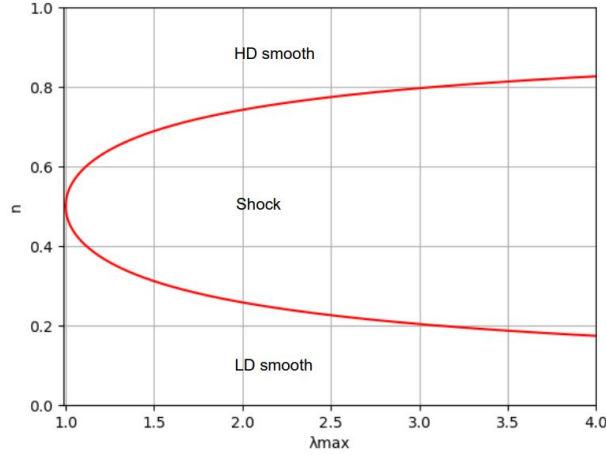


Figure 18: Phase diagram of the weak repulsion regime for $\lambda_{min} = 1$. The two branches (upper and lower) show the trends of n_+ and n_- with respect to λ_{max} .

As mentioned at the beginning of this section, we would like to compare the profiles we obtained under the assumption of a weak repulsion between neighboring particles with the ones corresponding to the steady state of the system in presence of non-interacting particles, hence we set $r = 1$ and $q = 1$. The results corresponding to this choice of the parameters, computed for two different values of the average density, are shown in Figure 19.

The qualitative behaviour of the steady state is exactly the same we analyzed before. The system is found in a shock phase if the value of the average density becomes sufficiently close to 0.5 and in a smooth phase otherwise. The main effect of introducing a repulsive interaction between particles in this regime is observed in the smooth phase, in which particles experiencing repulsion tend to enhance the density in proximity of the minimum of the function $\lambda(x)$ and reduce it close to the position of the maximum (Figure 20a).

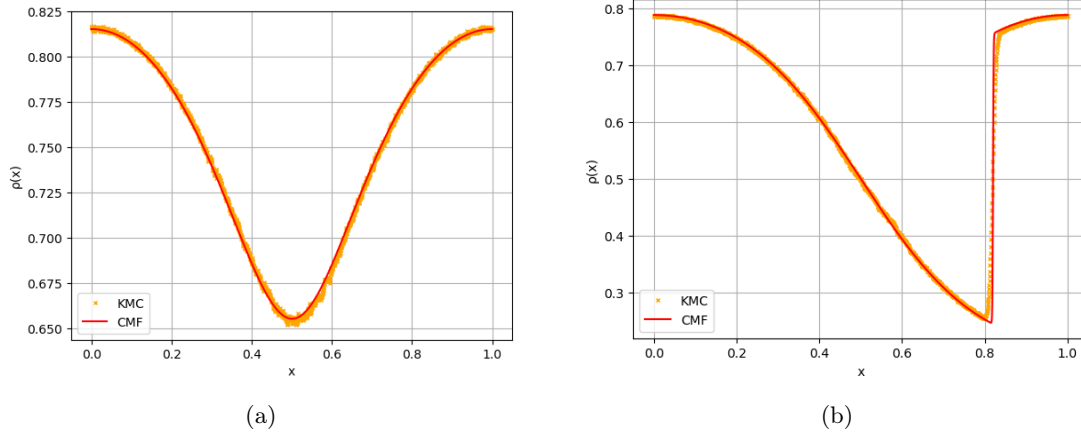


Figure 19: Stationary profiles for $q = r = 1$ corresponding to $n = 0.75$ (a) and $n = 0.6$ (b).

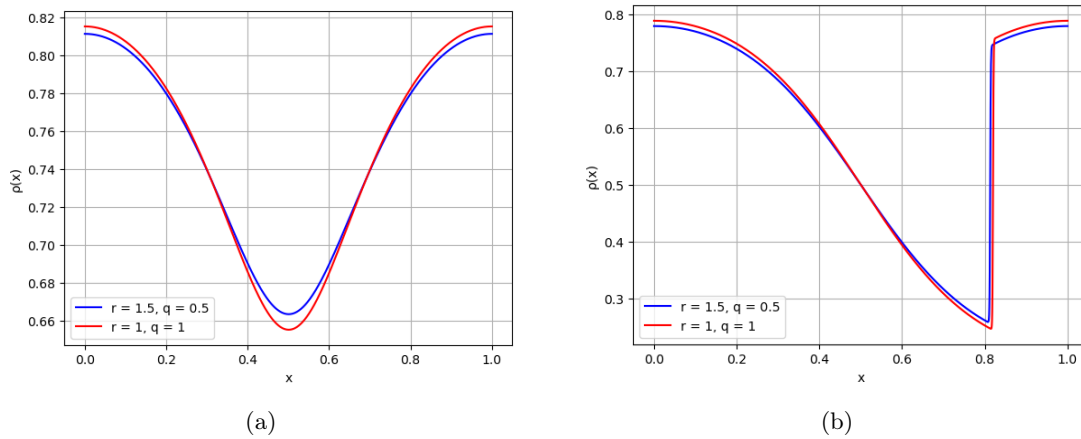


Figure 20: Comparison between the stationary profiles (obtained through CMF) corresponding to weakly repulsive particles ($r = 1.5, q = 0.5$) and non-interactive particles ($r = q = 1$) obtained for $n = 0.75$ (a) and $n = 0.6$ (b).

4.2 Strongly repulsive regime

As previously mentioned, when r becomes greater than the threshold value $r_f(q)$, two intermediate density analytical solutions (which will be denoted as $\rho_{2,\pm}(x)$) begin to emerge, and the steady state of the system is expected to show a different behaviour from a qualitative point of view.

In this case we decide to set $q = 0.05$, which implies $r = 1.95$ (the critical value is $r_f(0.05) \simeq 0.076$). This regime is particularly interesting since a new phenomenology of profiles is encountered when the intermediate density analytical solutions extend over the whole interval $[0, 1]$. We also find a peculiar "minimal current" phase for average density values in proximity of 0.5, which is something expected since a similar phase has been previously pointed out in the literature for the homogeneous TASEP with OBCs under the KLS assumption for the rates [4].

We will start by considering the features of the steady state in the case in which these solutions do not exist over the entire interval, but only over a restricted domain around the middle point $x = 0.5$, that is observed as long as $\lambda_{max} > \lambda_t(q, r)$ (in our case $\lambda_t = 1.35648$, so $\lambda_{max} = 1.5$ fulfills the previous inequality). The right border of this domain (which is the rightmost point of the interval over which the analytical solutions $\rho_{2,\pm}(x)$ are real) will be denoted as $x_r \in (0.5, 1)$ (by symmetry, the left border takes value $x_l = 1 - x_r$). Then, we will set $\lambda_{max} = 1.2$ and move to the other case.

4.2.1 Strongly repulsive regime for $\lambda_{max} > \lambda_t$ (multi-shocks regime)

For a sufficiently high (or low) value of the average density n , the system is found in a smooth phase whose features are analogous to the ones analyzed in the case of weak repulsion.

Conversely, as the average density approaches values which are closer to 0.5, the scenario becomes more complex, since several different shock phases are observed. Indeed, depending on the value of n , the stationary density profiles are characterized by one or more than one shock (up to a maximum of three), as one can see in Figure 21. For this reason, we will refer to this regime as the "multi-shocks regime" in the following.

Similarly to the weakly repulsive regime, the stationary current in each shock phase is maximal and for this choice of r and q corresponds to $J_{max} = 0.18255$.

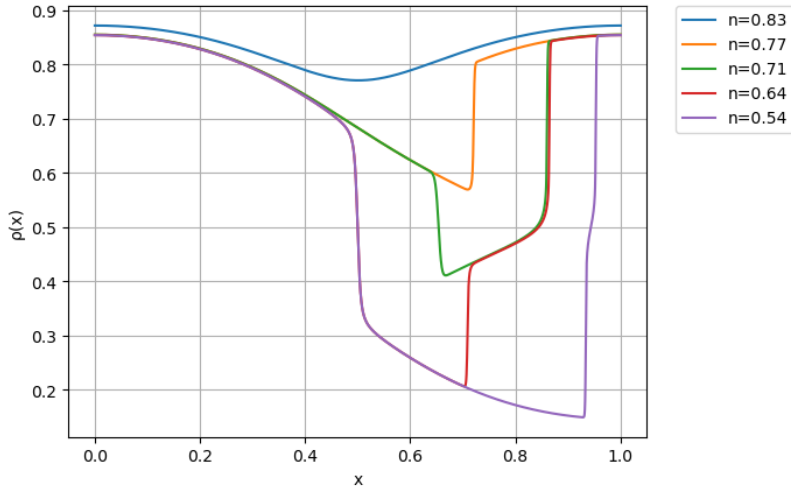


Figure 21: Stationary density profiles obtained with numerical CMF for different values of the average density n .

In the following, we would like to describe in details the different phases we have just mentioned. The stationary profiles belonging to the *HD* smooth phase corresponds to the analytical solution $\rho_{1,+}(x; J)$ obtained for $J \leq J_{max}$ (Figure 22).

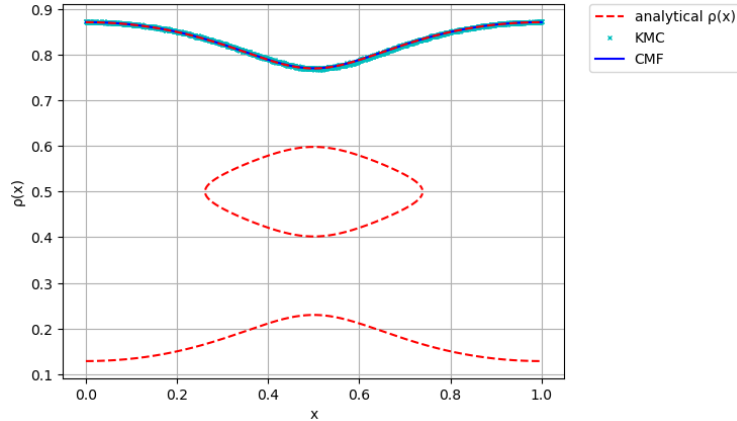


Figure 22: Comparison between stationary density profiles obtained for $n = 0.83$ and analytical solutions corresponding to $J = 0.16586$.

As in the case of weak repulsion, one can easily obtain the value of n determining the transition between the *HD* smooth phase and the subsequent shock phase (which will be denoted as $n_{1,+}$) by integrating the analytical solution $\rho_{1,+}(x; J_{max})$:

$$n_{1,+} = \int_0^1 \rho_{1,+}(x; J_{max}) dx. \quad (56)$$

When the average density becomes lower than $n_{1,+}$, the steady state of the system becomes a combination of the analytical solution $\rho_{1,+}$ and $\rho_{2,+}$ (similarly to what happens in the shock phase of the weakly repulsive regime with ρ_+ and ρ_-), with a single domain wall from the intermediate density solution to the high density one (Figure 23). Since $\rho_{2,+}$ is defined only for $1-x_r < x < x_r$, as the average density n decreases, one observes the position of the discontinuity in the corresponding profiles $\rho_n(x)$ moving rightward until it reaches x_r . For a further decrease of the average density, the system is no longer capable to fulfill particle conservation in a phase in which only $\rho_{1,+}$ and $\rho_{2,+}$ coexist. Hence, the system undergoes a phase transition to a new phase in which also the intermediate density solution $\rho_{2,-}$ coexists with the previous ones. This phase is characterized by two shocks, since one observes a jump discontinuity from density values corresponding to the $\rho_{2,+}$ solution to the $\rho_{2,-}$ ones and a subsequent transition to high density values, as one can see in Figure 24.

At the boundary between the 1-shock and 2-shocks phases, the stationary profile corresponds to the $\rho_{2,+}$ solution for $0.5 < x < x_r$ and to $\rho_{1,+}$ in the remaining portions of the $[0, 1]$ interval, so the average density value for which the transition between the two phases occurs is given by (setting from now on $\rho_{i,\pm}(x) \equiv \rho_{i,\pm}(x; J_{max})$ in order to simplify the notation)

$$n_{12,+} = \int_0^{1/2} \rho_{1,+}(x) dx + \int_{1/2}^{x_r} \rho_{2,+}(x) dx + \int_{x_r}^1 \rho_{1,+}(x) dx, \quad (57)$$

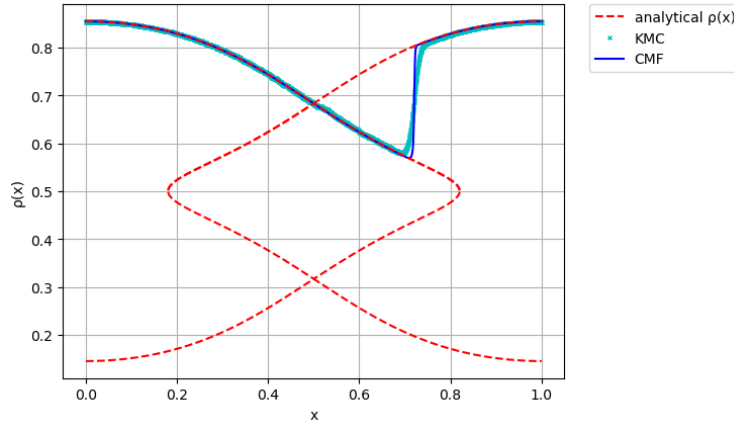


Figure 23: Stationary density profiles obtained for $n = 0.77$.

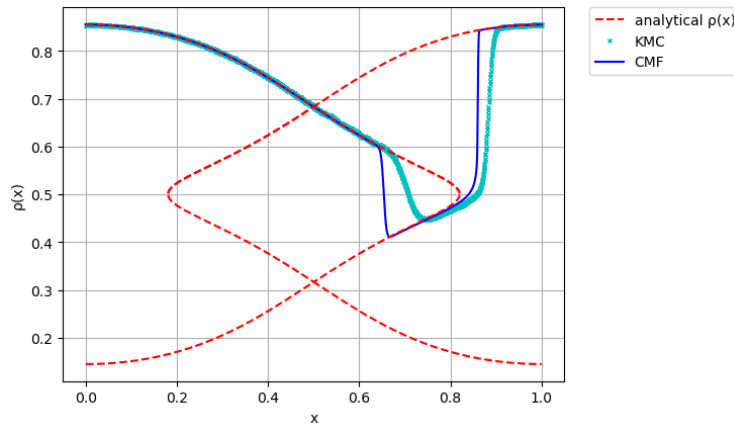


Figure 24: Stationary density profiles obtained for $n = 0.71$.

where the subscript of n specifies that this value of average density refers to the boundary between the 1-shock phase and the 2-shocks phase (moving n towards 0.5). In a similar way of what happens in the single shock phase, when the average density decreases in the range of values for which the system is found in the 2-shocks phase, the leftmost shock slides leftward in order to extend the region over which the stationary profile corresponds to $\rho_{2,-}$, until it reaches $x = 0.5$. At this point, in order to cope with a further decrease of n , the steady state profile moves from the $\rho_{2,-}$ solution to the $\rho_{1,-}$ one, giving rise to a new domain wall, which joins together the smooth portions corresponding to $\rho_{1,-}$ and $\rho_{2,-}$ and the system is found in a 3-shocks phase (Figure 25). For a values of n sufficiently close to 0.5, the second and third shocks merge giving rise to a single shock, and the system is found again in a 2-shocks phase in which only the high and low density analytical solutions ($\rho_{1,+}$ and $\rho_{1,-}$) coexist in the steady state (Figure 26).

As in the previous cases, one can compute explicitly the values of the average density at the boundary between the 2-shocks and the 3-shocks phase ($n_{23,+}$) and between the 3-shocks phase and the

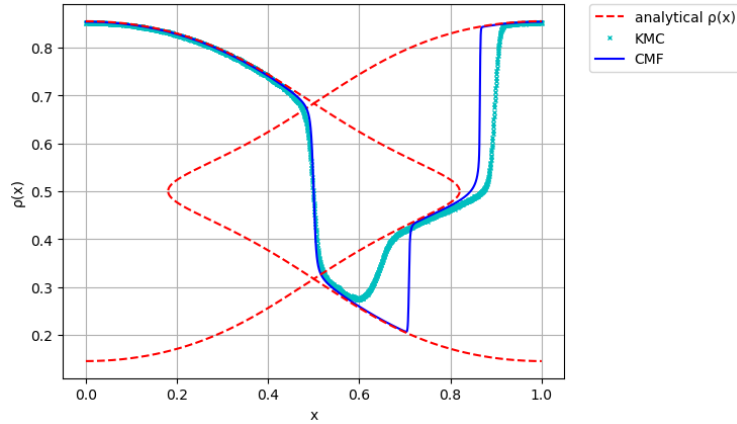


Figure 25: Stationary density profiles obtained for $n = 0.64$.

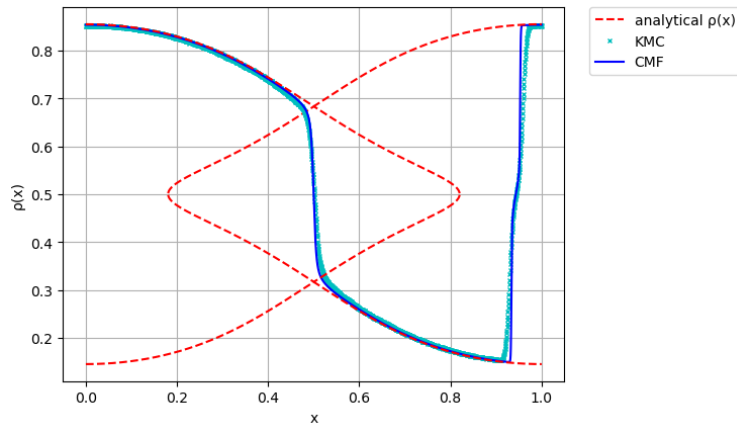


Figure 26: Stationary density profiles obtained for $n = 0.54$.

subsequent 2-shocks phase ($n_{32,+}$):

$$n_{23,+} = \int_0^{1/2} \rho_{1,+}(x) dx + \int_{1/2}^{x_r} \rho_{2,-}(x) dx + \int_{x_r}^1 \rho_{1,+}(x) dx, \quad (58)$$

$$n_{32,+} = \int_0^{1/2} \rho_{1,+}(x) dx + \int_{1/2}^{x_r} \rho_{1,-}(x) dx + \int_{x_r}^1 \rho_{1,+}(x) dx. \quad (59)$$

As one can see from Figures 24 - 25, the rightmost shock in the 2 and 3 shocks phases is placed at a slightly higher value of x with respect to the one predicted by the theory. Moreover, the profiles computed by means of KMC simulations exhibit shocks whose steepness decrease with the size of the jump discontinuity. As anticipated, these two discrepancies are consequences of the limited size of the system, and by increasing the number of lattice sites the stationary profiles obtained with both methods become progressively closer to analytical predictions (see Figures 27 - 28).

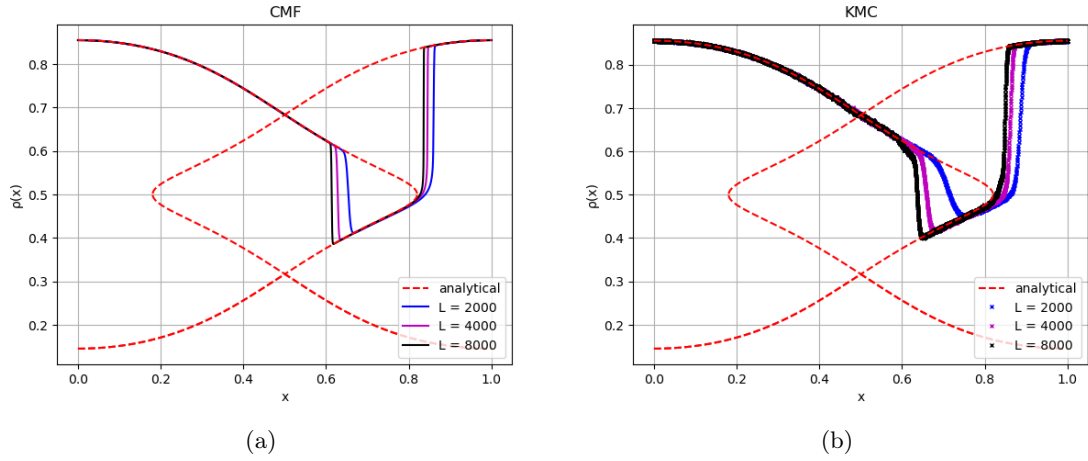


Figure 27: Comparison between the stationary profiles with $n = 0.71$ obtained for three different sizes of the lattice by means of CMF (a) and KMC (b).

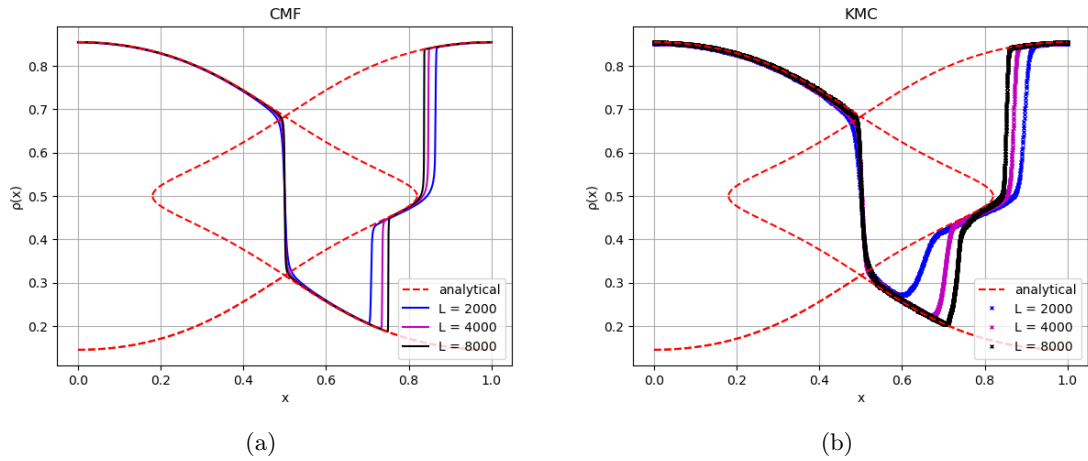


Figure 28: Comparison between the stationary profiles with $n = 0.64$ obtained for three different sizes of the lattice by means of CMF (a) and KMC (b).

For what concerns the profiles with $n = 0.54$, one can see that the two shocks are not perfectly merged into a single one for $L = 2000$. This is another finite size effect, actually if one increases the number of lattice sites to 8000 the alignment becomes almost perfect and the two single shocks are no longer distinguishable (Figure 29).

Before moving on with the discussion about the behaviour of the system for $\lambda_{max} < \lambda_t$, let us briefly describe the behaviour of the fundamental diagram in this regime.

From a qualitative point of view, the behaviour of $J(n)$ is the same as the one observed in the case of weak repulsion, with a plateau in correspondence of the maximal current, which extends over all the n values for which the system is found in a shock phase, and two lateral symmetric branches in which the current decreases as n approaches the boundary values, where the system is found in a

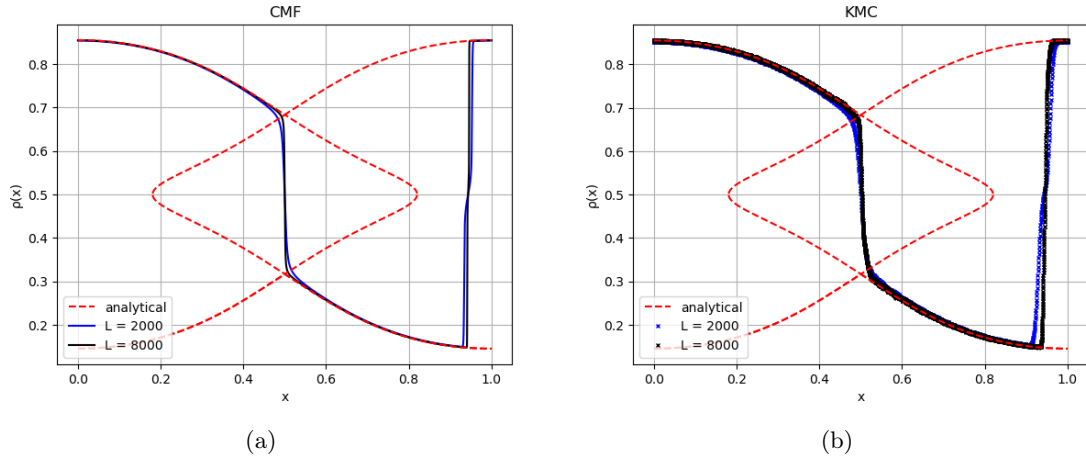


Figure 29: Comparison between the stationary profiles with $n = 0.54$ obtained for two different sizes of the lattice by means of CMF (a) and KMC (b).

smooth phase.

Conversely, the value of J_{max} and the breadth of the plateau depend on the strength of the repulsive interaction (Figure 30), since by decreasing q (which implies that the nearest neighbor repulsion is enhanced) one observes a decrease in the current value associated to a certain value of n and the range of n for which the current is maximal becomes wider.

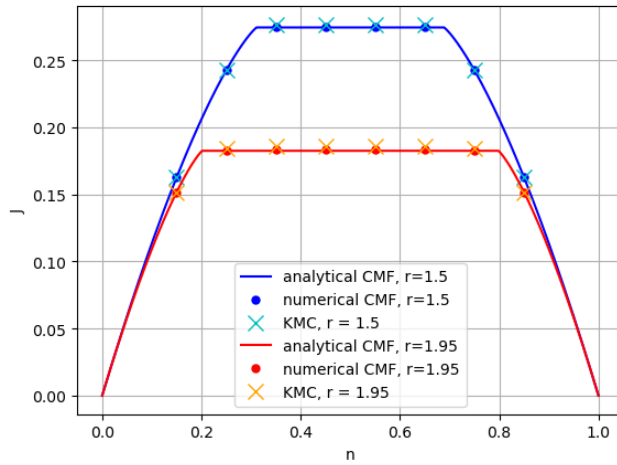


Figure 30: Fundamental diagram in the two regimes.

4.2.2 Strongly repulsive regime for $\lambda_{max} < \lambda_t$ (small shocks regime)

We would like to discuss in the following the steady state of the system when the ratio between the maximal and minimal value of the function $\lambda(x)$ describing the spatial modulation of the rates along the lattice becomes lower than the threshold value λ_t . In this case, we choose $\lambda_{max} = 1.2$

(remember that for our choice about the parameters r and q one obtains $\lambda_t = 1.35648$).

As previously mentioned, at odds with what has been observed for $\lambda_{max} = 1.5$, in this regime the analytical intermediate density solutions $\rho_{2,\pm}(x; J_{max})$ do not cross at the intermediate density value 0.5. As a consequence, we do not expect to find any shock phases with more than one shock when the steady state current of the system is maximal, since they are observed to emerge when more than two analytical solutions coexist in the corresponding stationary density profile.

A brief graphical description about the phenomenology of the steady state in this regime is shown in Figure 31.

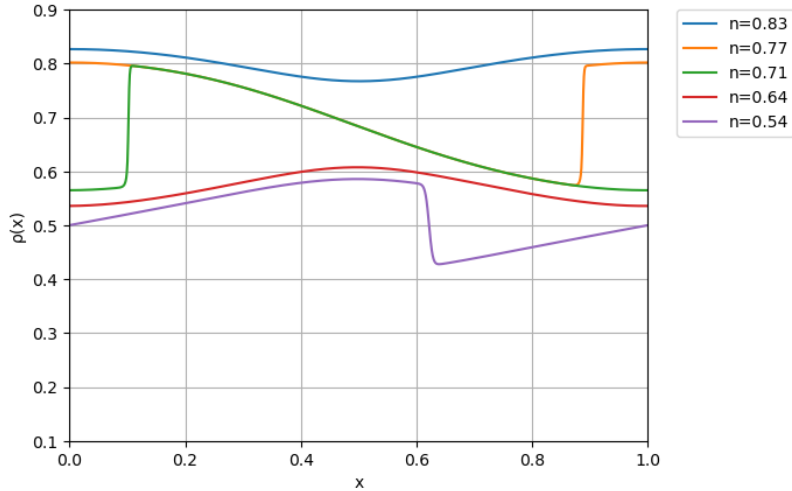


Figure 31: Stationary density profiles obtained with numerical CMF for different values of the average density n .

We decide to refer to this regime as the "small-shocks" one since the domain walls in this case are smaller in size with respect to the majority of the ones discussed within the previous regimes.

As in the previous case, for a sufficiently high value of the average density ($n > n_{1,+}$), the system is found in a smooth phase which corresponds to the analytical solution $\rho_{1,+}(x; J)$, with $J < J_{max}$ (Figure 32).

As n becomes lower than $n_{1,+}$, the steady state undergoes a transition into a maximal current shock phase in which the stationary profiles are given by a combination of $\rho_{1,+}(x; J_{max})$ and $\rho_{2,+}(x; J_{max})$ (Figure 33).

Interestingly, the phenomenology of the stationary profiles within this phase is similar to what is observed in the shock phase of the weakly repulsive regime for $n \in \{n_+, 1 - n_+\}$ (whose profiles were instead given by a combination of $\rho_+(x; J_{max})$ and $\rho_-(x; J_{max})$) and exhibit a kind of "symmetry" that resembles the one observed around $n = 0.5$ (Figure 34). This evidence is not surprising since the shape of the function $f(\rho)$ around the positions of the maxima in the case of strong repulsion reminds the local shape of the single maximum one around $\rho = 0.5$ (Figure 35), and this parallelism is reflected on the behaviour of the analytical solutions.

When the average density becomes lower than the integral of the analytical solution $\rho_{2,+}(x; J_{max})$ (whose corresponding value will be denoted as $n_{2,+}$), the steady state of the system is found again in a smooth phase, in which the stationary profiles match the analytical solutions $\rho_{2,+}(x; J)$ with $J \leq J_{max}$ (Figure 36) (this phase and the symmetric low density one will be denoted as HD_1 smooth

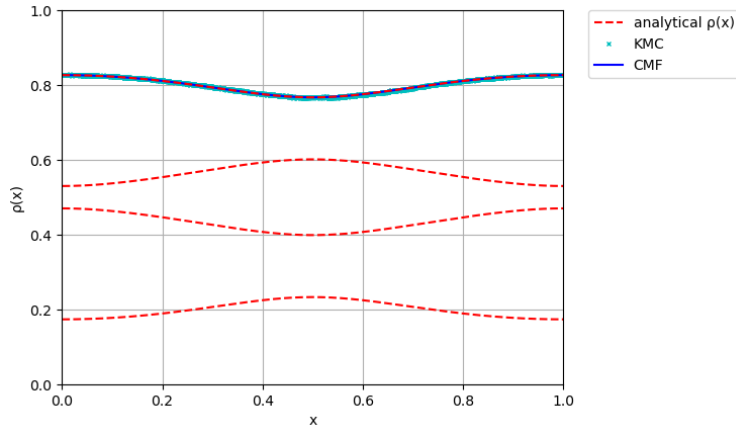


Figure 32: Comparison between stationary density profiles obtained for $n = 0.80$ and analytical solutions corresponding to $J = 0.16699$.

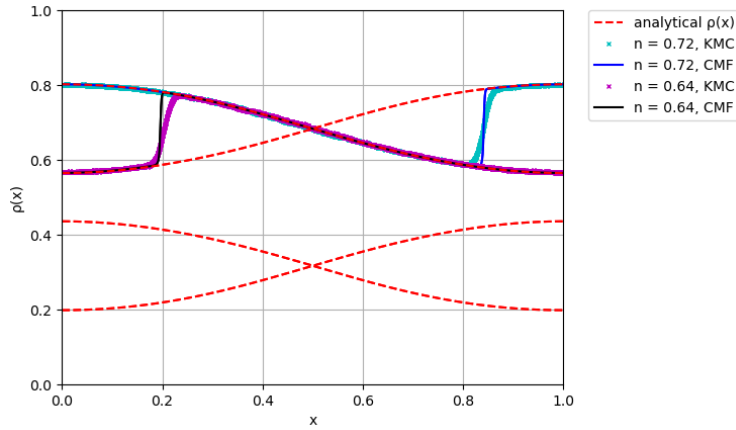


Figure 33: Stationary density profiles obtained for $n = 0.72$ and $n = 0.64$.

phase and LD_1 smooth phase respectively).

As the average density moves towards $n = 0.5$, the steady state current decreases until it reaches the minimal current $J_{min} = \lambda_{max} f_{min}$, where f_{min} is the local minimum of the current-density relation (due to our choices for the values of r , q and λ_{max} , one gets $J_{min} = 0.16149$). At this point, the stationary profiles of the system correspond to $\rho_{2,+}(x; J_{min})$, which means that the n value for which the steady state current becomes equal to J_{min} is given by

$$n_{2',+} = \int_0^1 \rho_{2,+}(x; J_{min}) dx. \quad (60)$$

For $n < n_{2',+}$, the system is found in a shock phase in which the steady state current is equal to J_{min} (for this reason we will refer to this phase as the minimal current shock phase) and the two intermediate density solutions $\rho_{2,+}(x; J_{min})$ and $\rho_{2,-}(x; J_{min})$ coexist in the corresponding station-

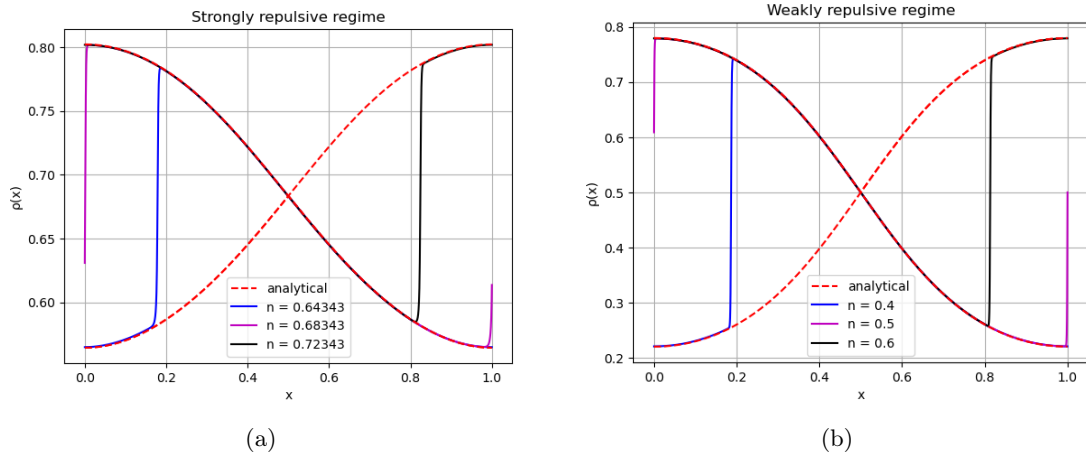


Figure 34: Comparison between the profiles obtained for $r = 1.95$, $q = 0.05$, $\lambda_{max} = 1.2$ (a) and $r = 1.5$, $q = 0.5$, $\lambda_{max} = 1.5$ (b) for n taking values in proximity of the maxima of the corresponding bulk current-density relations $f(\rho; r, q)$.

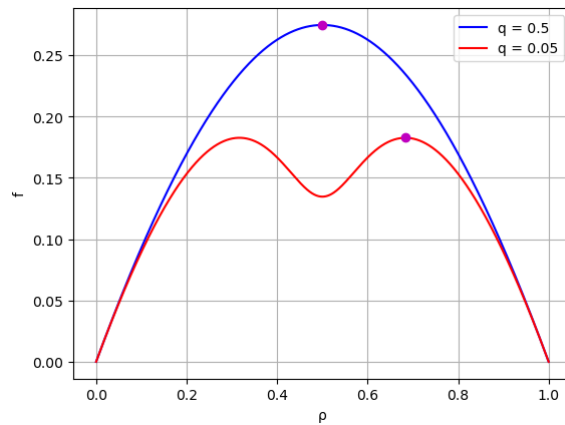


Figure 35: $f(\rho)$ in the weakly and strongly repulsive regimes.

ary density profiles (Figure 37).

Notice that, since an intermediate density smooth phase and a minimal current shock phase has been observed within this regime, the behaviour of the fundamental diagram is expected to be different also from a qualitative point of view with respect to the weakly repulsive regime. Consistently with the results discussed before, the diagram exhibits two symmetric lateral plateaus at $J = J_{max}$, which correspond to the maximal current shock phases, and a central one at $J = J_{min}$ in correspondence of the minimal current shock phase, that are connected by two branches over which the system is found in the intermediate density smooth phases.

As λ_{max} approaches λ_t , the values of J_{min} becomes progressively closer to J_{max} and the central plateau tends to align with the lateral ones (Figure 38).

Similarly to what has been done in the case of the weakly repulsive regime, one can build the phase diagram of the strongly repulsive regime by computing the values of the average densities that iden-

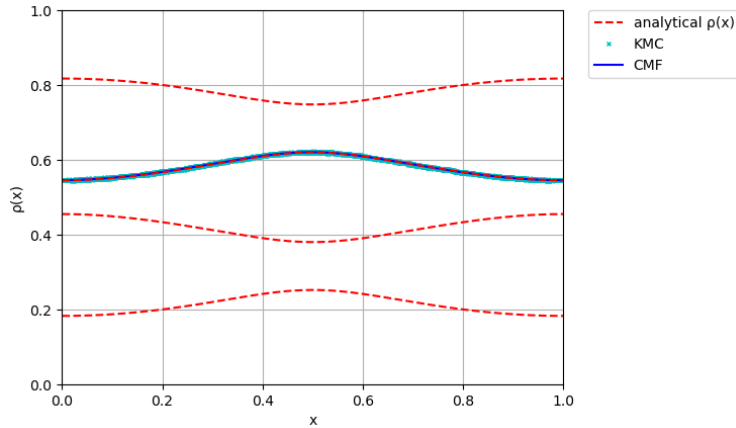


Figure 36: Stationary density profiles obtained for $n = 0.58$ with the analytical solutions corresponding to $J = 0.17312$.

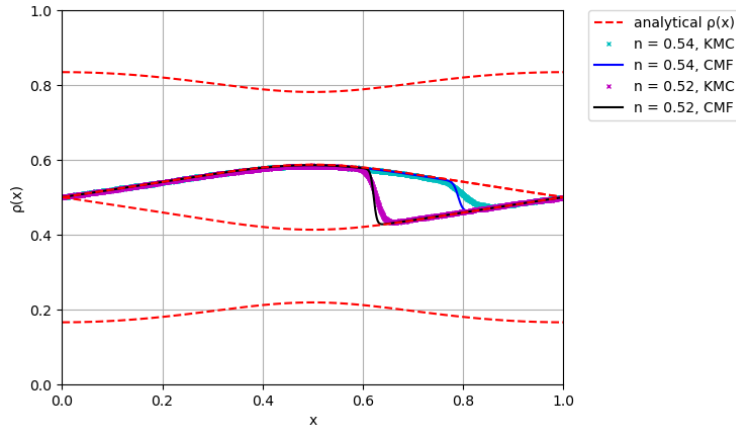


Figure 37: Stationary density profiles obtained for $n = 0.54$ and $n = 0.52$ with the analytical solutions corresponding to $J = J_{min}$.

tify the boundaries between the various phases for a certain range of values of λ_{max} (Figure 39). We restricted the description to $0.5 \leq n \leq 1$, since the phase diagram for $0 \leq n \leq 0.5$ is just the symmetric of this one with respect to the $n = 0.5$ axis).

Under the KLS condition ($r = 2 - q$), the function λ_t is decreasing with respect to q , which implies that, for a certain value of λ_{max} , one can move from the multi-shocks regime to the small shocks one by decreasing the value of q (in this sense, the latter can be regarded as a "very strongly" repulsive regime). This argument is quite relevant since we can confirm the predictions about the existence of a double-hump structure of the fundamental diagram for a sufficiently strong repulsive interaction, which have been pointed out by some previous works [6].

At this point, we can include both the weakly and strongly repulsive regime in a unique phase diagram in the (q, n) plane, which is described in Figure 40.

In the region over which the system is found in the weakly repulsive regime, one observes that there

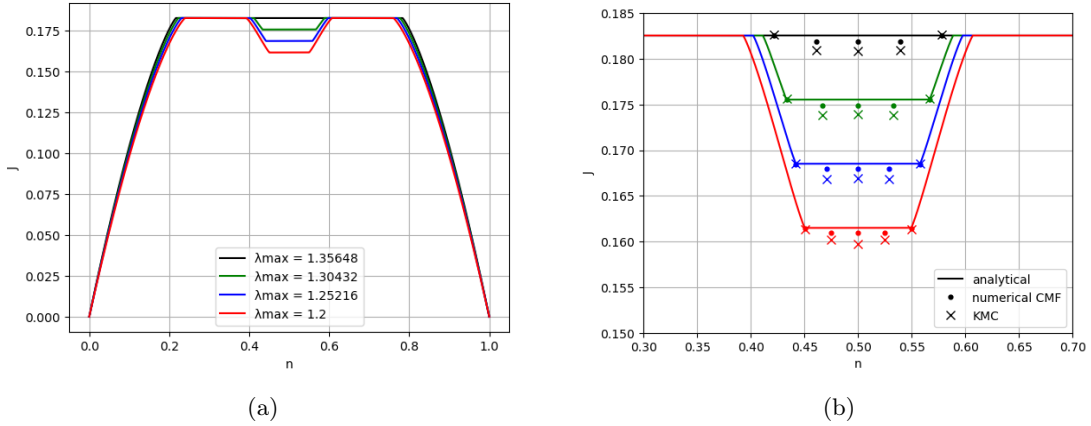


Figure 38: Comparison between the fundamental diagrams obtained for equally spaced values of λ_{max} between 1.2 and $\lambda_t = 1.35648$ (a), with a closer look in proximity of the central plateau (b). Notice that for $\lambda_{max} = \lambda_t$ one recovers the single plateau at $J = J_{max}$.

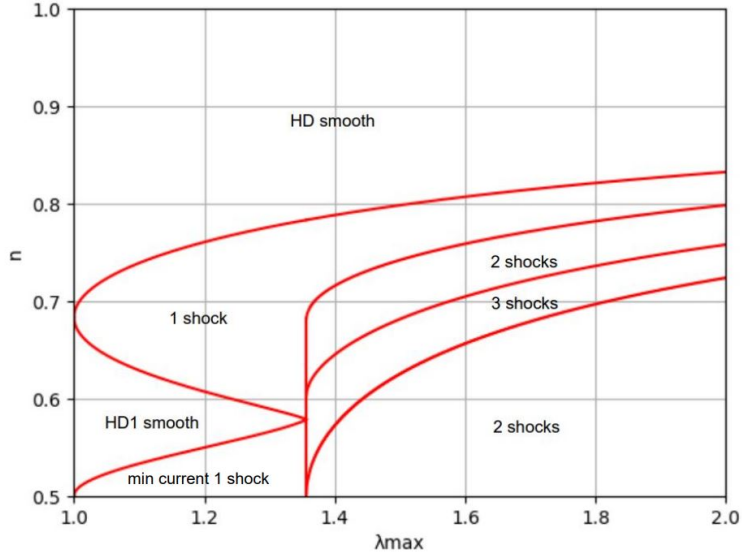


Figure 39: Phase diagram of the strongly repulsive regime.

is a certain value of q for which the breadth of the smooth region is maximal.

This result is consistent with the observation of a value of the interaction strength, within this regime, for which J_{max} is maximal [14].

For what concerns the strongly repulsive region, the minimal current phase becomes tighter as q decreases, since the minimal current allowed in the system becomes progressively smaller (this can be understood by looking at the current-density relation for different values of q , as one can see in Figure 41a). As a consequence, the intermediate density analytical solutions $\rho_{2,\pm}(x; J_{min}(q))$ tend to overlap in the limit $q \rightarrow 0$ (Figure 41b), and the HD_1 and LD_1 smooth phases merge together

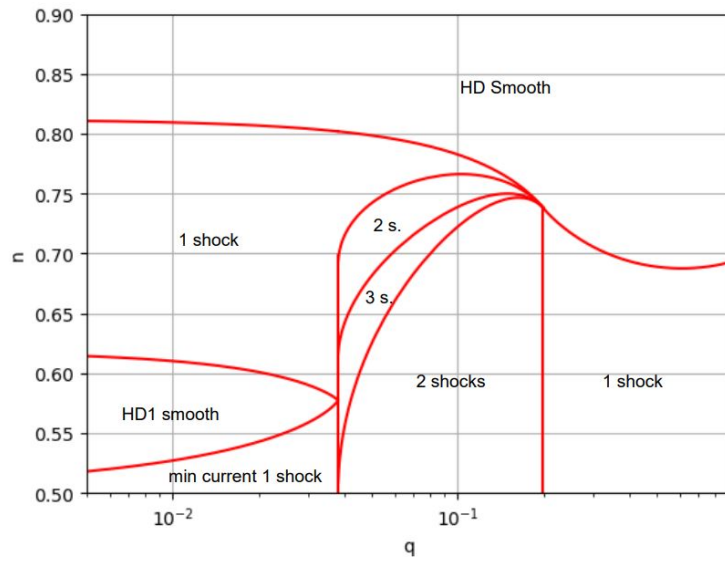


Figure 40: Phase diagram in the (q, n) plane for $\lambda_{max} = 1.5$ and $n > 0.5$.

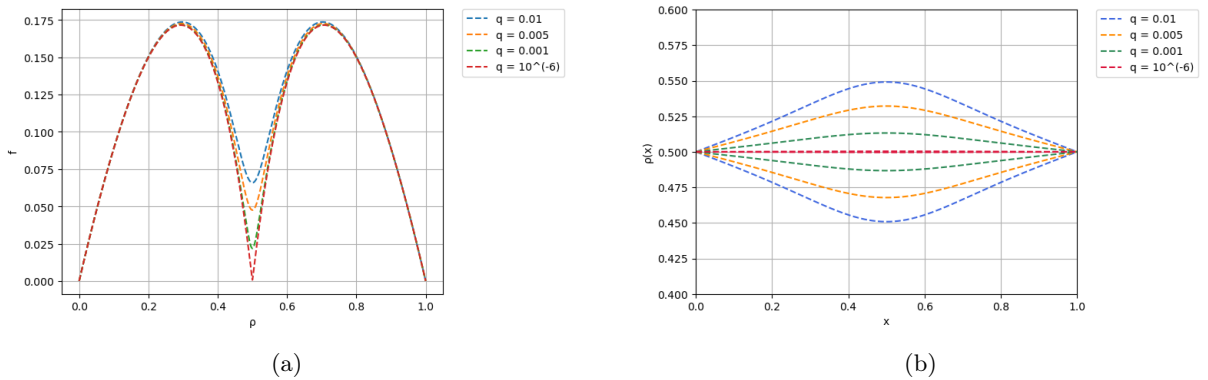


Figure 41: Comparison between the shapes of $f(\rho)$ for different values of q in the small shocks regime (a), with the corresponding intermediate density analytical solutions (b).

giving rise to a unique intermediate density smooth phase. In this limit, when the average density becomes equal to 0.5, no transport is allowed in the system ($J = 0$) since the steady state gets stuck into the configurations in which the occupied sites are located between two empty ones and vice versa, making the hopping of a particle extremely unlikely.

5 Conclusions

In this thesis we have considered an analytical theory based on the pair approximation combined with numerical methods to investigate the role of nearest neighbor repulsion in determining the macroscopic behaviour of the steady state of a TASEP model with quenched hopping rates and periodic boundary conditions.

We have found that, if the repulsion is sufficiently weak, the fundamental diagram and the behaviour of the stationary density profiles are basically the same as the ones which are observed in the case of non-interacting particles, at least from a qualitative point of view.

Conversely, for a sufficiently strong repulsion, one observes a qualitative change in the shape of the current-density relation that also affects the behaviour of the steady state.

Moreover, depending on the ratio between the minimal and maximal values of the function $\lambda(x)$, which regulates the rates modulation along the lattice, one can distinguish two different phenomenologies: a multi-shock regime, which displays several shock phases characterized by maximal current in which two or more analytical solutions coexist, and a small shocks regime, in which one observes two intermediate density smooth phases and a minimal current shock phase for an average density value sufficiently close to 0.5.

The same phenomenological picture can be portrayed by keeping constant the ratio between the maximal and minimal values of $\lambda(x)$ and instead considering variations of the parameter q in a proper interval (with $r = 2 - q$).

By means of these evidences we clarified that in the case of strong repulsion the phenomenology of the model is determined by the relationship between the ratios of some key parameters describing the degree of heterogeneity ($\lambda_{max}/\lambda_{min}$) and the quantitative behaviour of the current-density relation in proximity of intermediate density values (f_{max}/f_{min}).

The results we obtained under the KLS condition for the rates are really convincing and the profiles corresponding to KMC simulations are in very good agreement with the predictions of CMF obtained with both analytical and numerical methods, taking also into account the effect of finite size.

In addition to an accurate description of the phenomenology of the various shock phases we discussed in this work, the CMF approximation under the KLS condition turns out to be capable of predicting the slowly-varying portions of the stationary density profiles with great accuracy. This evidence suggests that the pair approximation (for which it has been shown that an exact bulk current-density relation can be found for a homogeneous system under this assumption) may prove to be exact in predicting the smooth regions of the stationary profiles even in the case of a heterogeneous model. This result is quite significant because it also implies that the phase diagram discussed at the end of the previous section may be exact, since it has been computed by integrating numerically the analytical solutions computed with the pair approximation.

When the KLS assumption is relaxed, one observes an evident increase of the mismatch between the profiles obtained with the two methods, and the pair approximation, besides some discrepancies at the level of the single profiles, in some cases seems no longer capable of predicting accurately the phase or the regime in which the system is found (in the following examples we will adopt the constraint $r = 1/q$).

In Figure 42 we report the profiles corresponding to $q = 0.1$, for which the system is expected to show the qualitative behaviour of the multi-shock regime. The profiles obtained with numerical CMF suggest that the system for $n = 0.75$, $n = 0.72$ and $n = 0.65$ should be in a 1, 2 and 3 shocks

phase respectively, while in the KMC results one observes 2 shocks in the first and third case and 3 shocks in the second one (which become more evident by increasing the lattice size, as shown in Figure 43).

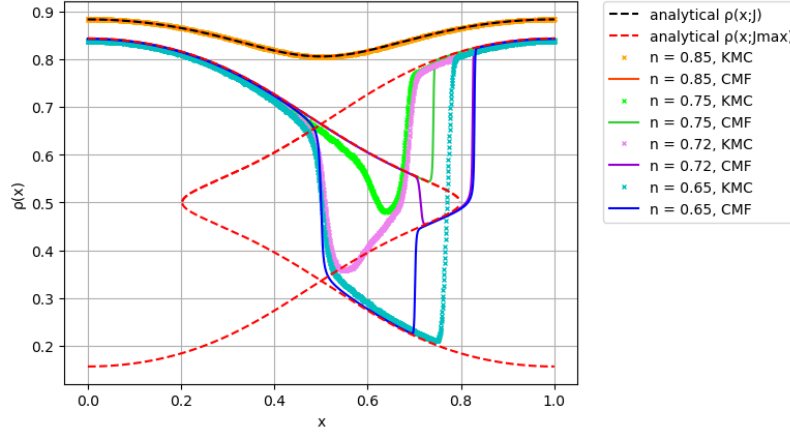


Figure 42: Comparison between the stationary profiles and the analytical solutions obtained for $q = 0.1$ and $r = 10$ with $J = 0.15604$ and $J_{max} = 0.19900$.

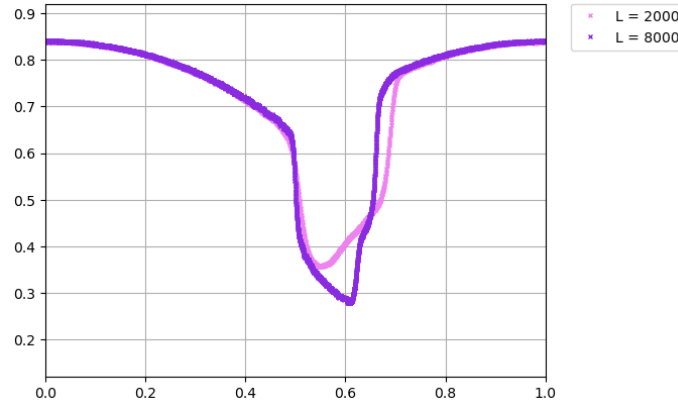


Figure 43: Comparison between the stationary profiles obtained for $q = 0.1$ and $r = 10$ with KMC simulations for two different lattice sizes.

If one sets $q = 0.05$, increasing the strength of the repulsion, the stationary profiles (and analytical solutions) obtained by CMF are the kind of ones which are observed in the small shocks regime, while the KMC profiles are still referable to the multi-shocks regime, as one can see in Figure 44 (for a further increase of the interaction strength, one recovers the qualitative behaviour of the small shocks regime also in the case of KMC simulations, with some mismatches at the level of the smooth portions of the intermediate density regions (Figure 45)).

Notice that these discrepancies are consistent with the observed mismatches between profiles of KMC simulations and the analytical solutions predicted by CMF at intermediate densities, since the boundaries between the various phases are defined through the latter.

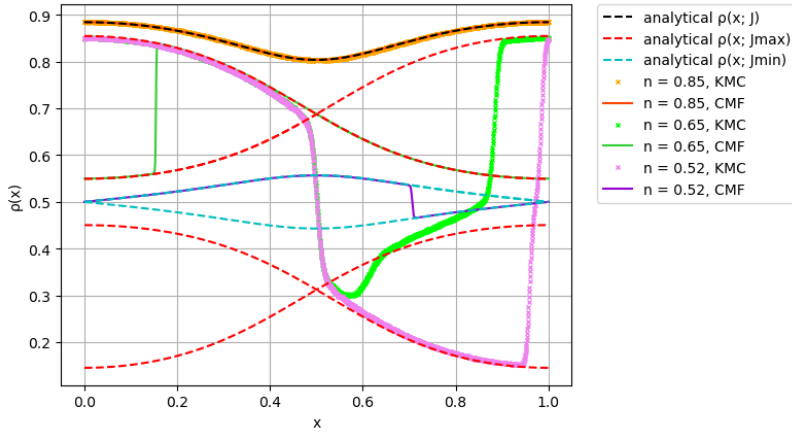


Figure 44: Comparison between the profiles and the corresponding analytical solutions obtained for $q = 0.05$ and $r = 20$ ($J_{max} = 0.18445$, $J_{min} = 0.12957$ and $J = 0.15298$).

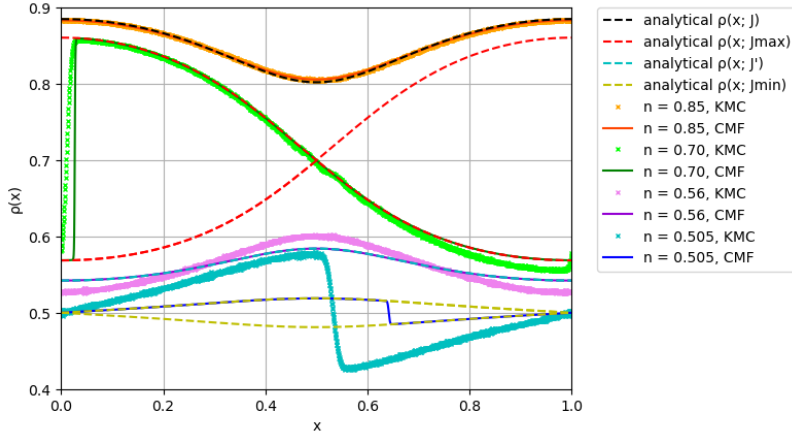


Figure 45: Comparison between the profiles and the corresponding analytical solutions for $J_{max} = 0.17654$, $J = 0.15096$, $J' = 0.13193$ and $J_{min} = 0.05654$, obtained for $q = 0.02$ and $r = 50$.

In particular, the results reported in Figure 42 suggests that, in the absence of the KLS condition, the CMF theory fails in predicting the position of the "coalescence point", where the two intermediate density solutions merge and then disappear.

In conclusion, we have shown that, under a particular choice for some key parameters (KLS condition), a mean-field-like semi-analytical theory is capable of describing in a basically exact way an absolutely non-trivial phenomenology which emerges when the spatial modulation of the hopping rates and the nearest neighbor repulsive interaction are simultaneously included in the model.

Moreover, even if one observes a significant deviation between the predictions of CMF theory and KMC simulations when the KLS condition is relaxed, the phenomenology of the model we described under this assumption seems to be rather "universal", being only related to the occurrence of a

bimodal shaped current-density relation.

We have not proven the exactness of our results, but the KMC outcomes discussed within this work provide a reliable numerical evidence in support of this hypothesis, and we are quite confident about this possibility.

References

- [1] C. T. MacDonald, J. H. Gibbs, and Pipkin A. C. “Kinetics of biopolymerization on nucleic acid templates”. In: *Biopolymers* 6 (1968), pp. 1–5.
- [2] A. Schadschneider, D. Chowdhury, and K. Nishinari. *Stochastic Transport in Complex Systems: From Molecules to Vehicles*. 2010.
- [3] B. Alberts et al. *Molecular biology of the cell, 4th edition*.
- [4] J. Hager et al. “Minimal current phase and universal boundary layers in driven diffusive systems”. In: *Physical review. E, Statistical, nonlinear, and soft matter physics* 63.056110 (2001).
- [5] M. Dierl, M. Einax, and P. Maass. “One-dimensional transport of interacting particles: Currents, density profiles, phase diagrams, and symmetries”. In: *Physical review E, Statistical, nonlinear, and soft matter physics* 87.062126 (2013).
- [6] B. Pal and A. K. Gupta. “Role of interactions in a closed quenched driven diffusive system”. In: *Journal of Physics A: Mathematical and Theoretical* 54.025005 (2021).
- [7] H. Hinsch, R. Kouyos, and E. Frey. “From Intracellular Traffic to a Novel Class of Driven Lattice Gas Models”. In: *Traffic and Granular Flow'05* (2007), pp. 205–222.
- [8] R. K. P. Zia, J. J. Dong, and B. Schmittmann. “Modeling Translation in Protein Synthesis with TASEP: A Tutorial and Recent Developments”. In: *Journal of Statistical Physics* 144 (2011), pp. 405–428.
- [9] Beatrice Mina. “Stochastic transport of interacting particles: a heterogeneous 1-dimensional model”. PhD thesis. Politecnico di Torino, 2022.
- [10] T. Banerjee and A. Basu. “Smooth or Shock: Universality in closed inhomogeneous driven single file motions”. In: *Physical Review Research* 2.013025 (2020).
- [11] A. Pelizzola, M. Pretti, and F. Puccioni. “Dynamical Transitions in a One-Dimensional Katz–Lebowitz–Spohn Model”. In: *Entropy* 21.11: 1028 (2019).
- [12] D. T. Gillespie. “Exact stochastic simulation of coupled chemical reactions”. In: *The Journal of Physical Chemistry* 81 (1977), pp. 2340–2361.
- [13] H. Teimouri, A. B. Kolomeisky, and K. Mehrabiani. “Theoretical analysis of dynamic processes for interacting molecular motors”. In: *Journal of Physics A: Mathematical and Theoretical* 54.065001 (2015).
- [14] T. Midha, A. B. Kolomeisky, and A. K. Gupta. “Effect of interactions for one-dimensional asymmetric exclusion processes under periodic and bath-adapted coupling environment”. In: *Journal of Statistical Mechanics: Theory and Experiment* 043205 (2018).